Down-regulation of Stathmin Is Required for the Phenotypic Changes and Classical Activation of Macrophages*

Kewei Xu[1] and Rene E. Harrison[2]

From the Departments of Cell and Systems Biology and Biological Sciences, University of Toronto Scarborough, Toronto, Ontario M1C 1A4, Canada

Background: Macrophage activation involves pronounced microtubule (MT) stabilization.
Results: Stathmin is degraded to enhance MT stabilization and allow robust activation in IFNγ-LPS-stimulated macrophages.
Conclusion: MT stabilization by reduced stathmin levels is required for enhanced phagocytosis, signal transduction, and activation of macrophages.
Significance: Understanding the nature and mechanisms of MT stabilization in activated macrophages is important for both immunology and cell biology fields.

Macrophages are important cells of innate immunity with specialized capacity for recognition and elimination of pathogens and presentation of antigens to lymphocytes for adaptive immunity. Macrophages become activated upon exposure to pro-inflammatory cytokines and pathogenic stimuli. Classical activation of macrophages with interferon-γ (IFNγ) and lipopolysaccharide (LPS) triggers a wide range of signaling events and morphological changes to induce the immune response. Our previous microtubule (MT) proteomic work revealed that the stathmin association with MTs is considerably reduced in activated macrophages, which contain significantly more stabilized MTs. Here, we show that there is a global decrease in stathmin levels, an MT catastrophe protein, in activated macrophages using both immunoblotting and immunofluorescent microscopy. This is an LPS-specific response that induces proteasome-mediated degradation of stathmin. We explored the functions of stathmin down-regulation in activated macrophages by generating a stable cell line overexpressing stathmin-GFP. We show that stathmin-GFP overexpression impacts MT stability, impairs cell spreading, and reduces activation-associated phenotypes. Furthermore, overexpressing stathmin reduces complement receptor 3-mediated phagocytosis and cellular activation, implicating a pivotal inhibitory role for stathmin in classically activated macrophages.

As critical effector cells of the innate immune response, macrophages are phagocytic cells with specialized capacity for pathogen destruction and antigen presentation to cells of the adaptive immune system (1). Resident macrophages are gener-ally quiescent but can quickly become activated upon exposure to various inflammatory challenges that trigger a wide range of signaling events and morphological changes. The classical activation of macrophages is induced by exposure to interferon-γ (IFNγ), a pro-inflammatory cytokine, and pathogenic stimuli such as lipopolysaccharide (LPS) (1, 2). Early work has shown that IFNγ does not activate macrophages but serves instead as a priming molecule that increases cell sensitivity to LPS (3). LPS is a component of the outer membrane of Gram-negative bacteria (4, 5) and is a potent activator for a variety of mammalian cell types, including macrophages, monocytes, neutrophils, and intestinal endothelial cells (6). In LPS-responsive cells, toll-like receptor 4 (TLR4) is the major LPS receptor (7, 8). TLR4 signaling culminates in activation of the transcription factor NF-κB, which controls the expression of an array of inflammatory cytokine genes (9). The inhibitory IκB family proteins (IκBα, IκBβ, and IκBε) bind directly to the p65 and c-*Rel* dimers of NF-κB and suppress transcriptional activity (10). Therefore, the rate of IκBα degradation significantly affects NF-κB signaling after LPS stimulation in macrophages and monocytes (11, 12).

Upon stimulation, activated macrophages up-regulate inducible nitric oxide synthetase (iNOS)[3] that produces nitric oxide (NO) (13, 14) and is commonly used as a marker of classically activated macrophages. The production of NO in activated macrophages is correlated with host resistance and antimicrobial actions (15, 16). Moreover, the secretion of NO by macrophages upon activation suppresses harmful immune responses to prevent autoimmunity (17, 18). Upon IFNγ-LPS stimulation, classically activated macrophages also exhibit increased membrane ruffling (19), altered receptor expression (20), and antigen presentation (21). Membrane ruffles are involved in macropinocytosis and facilitate signal amplification in macrophages (22). Phagocytosis plays a crucial role in host defense by allowing macrophages to recognize, ingest, and

[3] The abbreviations used are: iNOS, inducible nitric-oxide synthase; BMDM, bone marrow-derived macrophages; Cdk1, cyclin-dependent kinase 1; CR3, complement receptor 3; MT, microtubule; sRBC, sheep red blood cell; PMA, phorbol myristate acetate; MTOC, MT-organizing center; PFA, para-formaldehyde; SEM, scanning electron microscopy; ANOVA, analysis of variance; KIS, kinase-interacting stathmin.

destroy invading pathogens. Complement receptor 3 (CR3) is a heterodimeric transmembrane glycoprotein consisting of CD11b associated with CD18 (23), which binds to and captures C3bi-opsonized particles (24). Interestingly, our previous work has demonstrated that IFNγ-LPS-induced membrane ruffles participate in capture of C3bi-opsonized particles (19) showing a role for these membrane protrusions in both macropinocytosis and phagocytosis in IFNγ-LPS-activated macrophages.

Classical activation of macrophages is also characterized by pronounced stabilization of the microtubule (MT) network (25–27). MTs are linear polymeric components of the cytoskeleton that are composed of α- and β-tubulin heterodimers (28, 29). MTs are asymmetric polar structures that are generally unstable due to constant shrinking and growing (30). MTs have a quickly growing and dynamic plus-end localized at the cell periphery and a slowly growing minus-end embedded in the MT-organizing center (MTOC) (31, 32). MTs are responsible for many cellular processes such as organelle localization, mechanical stability, motility, cell polarity, and chromosome separation (30). In general, MT formation in cells is driven by polymerization and depolymerization of tubulin subunits, and the stability of formed MTs is regulated by intrinsic tubulin GTPase activity and the involvement of microtubule-associated proteins (MAPs) (28, 29). Alteration of tubulin subunits occurs though post-translational modification, such as acetylation and tyrosination (33, 34), and stable MTs often contain acetylation on the conserved lysine 40 residue of α-tubulin (35), allowing acetylated tubulin to serve as a marker of stable MT subsets (36).

Our previous proteomic study of MT-binding proteins showed that classical activation of macrophages caused a reduction in stathmin association with MTs (37). Stathmin/oncoprotein 18 (Op18) is a highly conserved MT-destabilizing protein involved in many biological processes such as development and differentiation (38, 39). It was first identified as a protein greatly overexpressed in leukemia and other solid tumors (40, 41) where high expression indicates poor prognosis (42). Stathmin destabilizes MT by sequestering tubulin subunits, which greatly reduces the amount of tubulin available for MT assembly (43). In addition, stathmin directly interacts with MTs by binding and destabilizing exposed protofilaments, to induce MT plus-end catastrophe (44). Because of its importance in various biological processes, stathmin activity is heavily regulated by different kinases on its four serine phosphorylation sites (serines 16, 25, 38, and 63). The phosphorylation of these serine residues deactivates the MT destabilizing activity of stathmin (43).

In this study, we examined whether there was a functional link between stathmin down-regulation and classical activation of macrophages. We first assessed whether stathmin protein was reduced globally in macrophages and examined the regulatory mechanisms responsible for its destruction. We examined the importance of stathmin down-regulation on MT stability, cell area, and shape by ectopically overexpressing stathmin-GFP in activated macrophages. We also characterized the impact of stathmin overexpression on membrane ruffle formation and complement receptor 3 (CR3)-mediated phagocytosis. Finally, we discovered that classical activation of

macrophages was impaired when stathmin levels were artificially increased, which was likely a result of reduced TLR4 cell surface targeting. These results show that stathmin down-regulation is key for MT stabilization and macrophage activation.

Experimental Procedures

Reagents, Antibodies, and Constructs—Dulbecco's modified Eagle's medium (DMEM) and fetal bovine serum (FBS) were purchased from Wisent Inc. (St-Bruno, Quebec, Canada). FuGENE-HD was purchased from Promega (Madison, WI). Lipopolysaccharide (LPS) from *Salmonella enterica* serovar *typhimurium*, interferon-γ (IFNγ), and myristate acetate (PMA) were purchased from Sigma. Alexa Fluor phalloidin and 4′-6-diamidino-2-phenylindole (DAPI) were obtained from Invitrogen. Antibodies were obtained as follows: rabbit polyclonal anti-stathmin, rabbit polyclonal anti-Cdk1, rat monoclonal anti-TLR4 antibody, rabbit monoclonal anti-IκBα antibody, and rabbit anti-phospho-Cdk1 (Thr-161) were from Abcam Inc. (Cambridge, MA). Rabbit polyclonal anti-phospho-stathmin (Ser-38) was from GeneTex (Irvine, CA). Mouse monoclonal anti-α-tubulin and anti-acetylated tubulin antibodies were obtained from Sigma. Rabbit polyclonal NF-κB antibody was purchased from Santa Cruz Biotechnology (Santa Cruz, CA). Corresponding rabbit, mouse, and rat monoclonal HRP and Cy2-, Cy3-, and Cy5-conjugated secondary antibodies were from Jackson ImmunoResearch (West Grove, PA).

For stathmin-GFP construction, total RNA was isolated from cultured RAW 264.7 cells using the RNeasy minikit from Qiagen (Hilden, Germany). The cDNA sequences of full-length stathmin were amplified with Superscript One-step RT-PCR with a platinum *Taq* kit using the following primer pairs: stathmin-F, 5′-aatgctagcaccaggcatcttctgatattcaggtgaaagagct-3′; stathmin-R, 5′-attgaattcggtcagcctcagtctcatccgcggg-3′. The resulting PCR products were cloned in-frame to pmEGFP-1 vectors (Addgene Plasmid, catalog no. 36409), using NheI and EcoRI restriction sites for stathmin.

Cell Culture, Transfection, and Mouse BMDM Isolation—The murine RAW 264.7 macrophage cell line was obtained from the American Type Culture Collection (Manassas, VA) and maintained at 37 °C and supplied with 5% CO_2 in DMEM supplemented with 10% heat-inactivated FBS. RAW 264.7 cells were grown to 70–80% confluence in tissue culture 6-well plates, with or without 25-mm glass coverslips. RAW 264.7 cells were transfected with stathmin-GFP or empty GFP vector and/or EB1-mCherry (45) using FuGENE HD (Promega), according to the manufacturer's instruction, with overnight incubations for plasmid expression. Stable cell lines were generated by selection with G418 (1 mg/ml) for 3 weeks before sorting with BD FACSAria III (BD Biosciences). For low and high stathmin-GFP overexpressors, stathmin-GFP-expressing cells were sorted based their GFP intensity. Top 5% (high overexpressors) and bottom 5% (low overexpressors) of the population were collected as discrete populations by BD FACSAria III (BD Biosciences). GFP fluorescence intensity was verified with immunofluorescence microscopy and flow cytometry. Mouse BMDM was harvested from long bones of adult mice. Cells were washed twice with PBS and then suspended in complete culture medium (RPMI 1640 with 100 IU/ml each of penicillin

and streptomycin and 10% heat-inactivated FBS). Cells were grown in tissue culture 6-well plates stimulated with M-CSF (100 ng/ml) at 37 °C with 5% CO_2 for 5–7 days, to allow for differentiation into macrophages. Viable cells were counted using a 0.4% trypan blue solution from Mediatech Inc. (Herndon, VA). All animal studies were conducted under protocols approved by the University of Toronto Committee on Use and Care of Animals.

Macrophage Activation and Pharmacological Treatments—Resting RAW 264.7 cells or differentiated mouse BMDM were classically activated by a combination of 100 ng/ml LPS and/or 100 units/ml IFNγ in FBS-free DMEM. For proteasome inhibition, RAW 264.7 cells were classically activated and treated with 10 μM MG-132 (Sigma) in the last 3 h of activation. For Cdk1 inhibition, RAW 264.7 cells were classically activated and treated with 10 μM RO3306 (Sigma) for the duration of activation (6 h).

Immunostaining and Fluorescent Imaging—Cells were fixed in 4% PFA for 20 min and permeabilized with 0.1% Triton X-100 in PBS containing 100 mM glycine for 15 min. For immunostaining of MTs, cells were fixed and permeabilized in ice-cold 100% methanol for 10 min at −20 °C. Cells were blocked in PBS with 5% FBS for 1 h and incubated with the indicated primary antibodies in PBS with 1% FBS for 1 h using the following dilutions: stathmin (1:250), α-tubulin (1:2000), acetylated α-tubulin (1:2000), TLR4 (1:1000), and NF-κB (1:300). Cells were then incubated with the corresponding fluorochrome-conjugated secondary antibodies (1:1000) in PBS with 1% FBS for 1 h. Where indicated, secondary antibodies were incubated together with Alexa Fluor phalloidin (1:500) to stain F-actin. Cells were mounted using Dako Fluorescent Mounting Medium (Dako Cytomation, CA). For nuclear staining, cells were washed twice with double distilled H_2O and incubated for 10 min with DAPI (1:10,000) before mounting. Cells were visualized under a ×63 oil immersion objective using an inverted Zeiss AxioObserver Z1 epifluorescent microscope using AxioVision software.

Immunoblotting and Densitometric Analysis—Total cell lysates were obtained by scraping cells in RIPA lysis buffer in the presence of protease and phosphatase inhibitor mixtures (Sigma). For immunoblotting, protein samples were boiled in Laemmli buffer for 10 min. An equal amount of protein was separated on 8 or 10% SDS-PAGE and transferred to nitrocellulose membranes (Bio-Rad). Blots were blocked for 1 h in TBST with 5% skim milk or 5% BSA (BioShop Canada, Ontario), and then incubated with the corresponding primary antibody overnight at 4 °C. The dilutions were as follows: stathmin (1:10,000), β-actin (1:10,000), iNOS (1:1000), phospho-stathmin (Ser-38) (1:1000), Cdk1 (1:1000), phospho-Cdk1 (Thr-161) (1:1000), TLR4 (1:1000), and IκBα (1:1000). Blots were incubated with the relevant peroxidase-coupled secondary antibodies (1:1000) for 1 h, and bound antibody was visualized using the Supersignal West Pico Chemiluminescent Substrate kit (ThermoScientific, MA), according to the manufacturer's instructions. Densitometry analysis of protein bands was conducted from independent experiments with ImageJ software (National Institutes of Health). Protein bands

subjected to densitometric analysis were not saturated or overexposed.

Live Cell Imaging of EB1 Comets and MT Nucleation Assay—For time-lapse imaging of MT growth, macrophages were co-transfected with EB1-mCherry and GFP or stathmin-GFP. Cells were activated with IFNγ-LPS for 6 h and mounted in a temperature-controlled stage heater set at 37 °C on an inverted Zeiss AxioObserver Z1 epifluorescent microscope using AxioVision software. Epifluorescent images were acquired for a period of 10 s at 1-s intervals. For EB1 comet quantification, time lapse sequences were advanced frame by frame, and EB1-mCherry comet emergence from the MTOC was counted.

Scanning Electron Microscopy (SEM)—GFP and stathmin-GFP-expressing macrophages grown on plastic Therma Nex coverslips were serum-starved for 1 h. Where indicated, cells were prestimulated with IFNγ-LPS (100 units/ml and 100 ng/ml, respectively) for 6 h or left unstimulated in serum-free DMEM (control). For ruffle analysis, cells were fixed immediately after 6 h of IFNγ-LPS stimulation and then washed with 0.1 M phosphate buffer (pH 7.4) followed by fixation with 2% glutaraldehyde. After washing with 0.1 M sodium cacodylated buffer, cells were postfixed with buffered 1% OsO_4 for 1 h and dehydrated in ethanol. The samples were then critical-point dried in liquid CO_2 and sputter-coated with gold. Images were acquired with a Hitachi S530 SEM.

C3bi-sheep Red Blood Cells (C3bi-sRBC) Binding Assays—C3bi opsonization was performed by incubating sRBCs with sub-agglutinating concentrations of IgM (1:10) (Cedarlane Labs, Ontario, Canada) in PBS with 0.5 mM $CaCl_2$ and $MgCl_2$ for 1 h at room temperature. Excessive IgM was washed off, and sRBCs were then incubated with C5-deficient serum (Sigma) for 30 min at 37 °C with frequent mixing. C3bi-opsonized sRBCs were then washed three times with PBS. For C3bi-RBC binding assays, GFP-expressing and stathmin-GFP-expressing cells were serum-starved for 1 h and then incubated with or without IFNγ-LPS stimulation for 6 h or 150 nM PMA for 15 min prior to the addition of excess C3bi-RBCs. C3bi-sRBCs were incubated with the cells for 10 min and then washed vigorously with PBS. Cells were fixed with 4% PFA in PBS and then C3bi-sRBCs were stained with a Cy3-conjugated secondary antibody and imaged with an inverted Zeiss AxioObserver Z1 epifluorescent microscope.

Flow Cytometry—For flow cytometry analysis, IFNγ-LPS-stimulated or -unstimulated GFP-expressing and stathmin-GFP-expressing macrophages were scraped from tissue culture flasks and washed twice with ice-cold PBS with 1% FBS. Cells were then fixed with 4% PFA for 20 min and blocked with PBS with 5% FBS for 1 h. Surface TLR4 was immunolabeled with 2 μg of rat monoclonal anti-TLR4 antibody (Abcam, Cambridge, MA) per 1.5×10^6 cells followed by Cy5 anti-rat secondary antibody. Surface staining of TLR4 was analyzed with LSR-Fortessa (BD Biosciences) and FACSDiva Software (BD Biosciences). Data analysis was conducted using FlowJo (TreeStar Inc.). The total population of viable cells was gated using forward and side scatter. The fluorescence of untreated cells was recorded to determine the level of background fluorescence for negative control cells. A total of 10,000 events for each sample were acquired individually in the "live-gate" mode. The results

were expressed as relative fluorescence intensity calculated as geometric mean fluorescence intensity of stimulated cells/geometric mean fluorescence intensity of control (unstimulated) cells. The experiment was repeated three times, and the expression levels were expressed as the mean ± S.E. Statistical significance was determined using the Student's *t* test.

Quantification and Statistical Analysis of Cell Spreading, Membrane Ruffling, Ruffle Length, C3bi-sRBC Binding, and NF-κB Distribution—RAW 264.7 cells expressing GFP and stathmin-GFP were classically activated, fixed, and stained with phalloidin for F-actin and DAPI and imaged by epifluorescence microscopy. For cell area measurements, ImageJ software was used. Specifically, cells of interest were selected manually using the drawing/selection tool and then areas of the cell were measured using the "MEASURE" function. $n > 50$ measurements were expressed as the mean ± S.E. Statistical significance was determined using the Student's *t* test.

For ruffle measurements, we defined membrane ruffles as F-actin-rich membrane protrusions on the dorsal surfaces of macrophages. To determine the average number of ruffles per macrophage, the number of discrete dorsal ruffles in each cell was tabulated for 100 macrophages and averaged. Images were acquired using the same fluorescence intensity and exposure time between treatments and replicates. Experimental values were presented as mean ± S.E. of the experimental triplicates. GraphPad Prism was used to perform ANOVA test of the data, with *p* values of <0.05 considered significant. To determine the length of membrane ruffles, individual ruffles were selected and traced manually using ImageJ software, and the length of membrane ruffles was acquired using the "MEASURE" function. $n > 50$ measurements were expressed as the mean ± S.E. Statistical significance was determined using the Student's *t* test.

For determining the C3bi-sRBC binding index, the number of C3bi-sRBCs bound per 100 macrophages was tabulated in PMA- and LPS-activated RAW 264.7, GFP, and stathmin-GFP-expressing cells. Values were presented as mean ± S.E. of three independent experiments. GraphPad Prism was used to perform ANOVA test evaluations of the data, with values of $p < 0.05$ considered significant.

For NF-κB distribution analysis, immunostaining patterns in cells were classified as cytoplasmic, diffuse, or nuclear based on the localization of NF-κB. We defined the "cytoplasmic" phenotype as cells with NF-κB localized in its cytosol and excluded from its nucleus, whereas the "diffuse" phenotype showed an evenly distributed NF-κB in both the cytosol and the nucleus. The "nuclear" phenotype described cells with NF-κB primarily localized in the nucleus and not the cytosol. The percentages of NF-κB phenotypes were calculated by dividing the specific localization pattern by the total cells scored. $n > 50$ per trial per time point, and the experimental values were presented as mean ± S.E. of three independent experiments. GraphPad Prism was used to perform ANOVA test evaluations of the data, with values of $p < 0.05$ considered significant.

Results

Stathmin Protein Levels Are Significantly Reduced in Classically Activated Macrophages—We previously observed pronounced reduction of MT-associated stathmin in IFNγ-LPS

stimulated macrophages (37). To assess whether this reflected reduced MT recruitment of stathmin or diminished total stathmin protein levels, we monitored stathmin levels from whole cell lysates of activated macrophages. IFNγ-LPS activated macrophages experienced increased cell spreading and MT network complexity as expected (25) (Fig. 1*A*), which we hereafter refer to as the activated phenotype. Immunofluorescent examination of stathmin levels showed a decrease in stathmin fluorescent intensity in activated macrophages, compared with unstimulated control cells (Fig. 1*A*).

To validate whether the decreased stathmin fluorescent intensity was due to total protein reduction, immunoblotting was used. We observed a sharp decrease in total stathmin protein levels upon IFNγ-LPS stimulation (Fig. 1*B*), and densitometric analysis normalized to actin levels showed a reduction of stathmin by 50% or more by 3 h (Fig. 1*C*). After 3 h, stathmin protein levels remained low in activated macrophages over an 18-h activation period (Fig. 1, *B* and *C*). To determine whether the reduction of stathmin was a common characteristic for classically activated macrophages, we examined stathmin expression in mouse BMDMs. Interestingly, BMDMs experienced a significant reduction in stathmin protein levels upon 6 h of IFNγ-LPS stimulation (Fig. 1, *D* and *E*).

Overall, our observations suggested a general trend of stathmin protein down-regulation in macrophages upon IFNγ-LPS stimulation. At 6 h post-stimulation, ~60% of cells were exhibiting the activated macrophage phenotype (data not shown). Because stathmin levels did not change significantly after 6 h, we used 6 h post-IFNγ-LPS stimulation as a peak activation point for all subsequent stathmin experiments.

Reduction of Stathmin Protein Levels in Activated Macrophages Is an LPS-dependent Response and Requires Functional Proteasomes and Activation of Cdk1—In fibroblast and cancer cells, stimulation with IFNγ promotes the down-regulation of stathmin protein by suppressing the transcription factor (E2F) for the stathmin gene (46, 47). Because classical activation of macrophages involves both IFNγ and LPS exposure, we wanted to tease out the relative contribution of these stimuli on stathmin protein down-regulation in activated macrophages. Macrophages were stimulated with either LPS or IFNγ for 6 h before lysate collection. In addition, RAW 264.7 cells were stimulated with IFNγ-LPS, or left unstimulated (positive control and negative control, respectively). Immunoblot analysis and densitometry quantification indicated that the reduction of stathmin protein levels in macrophages was LPS-dependent, as stimulation with LPS alone significantly reduced stathmin protein levels in a comparable manner to cells exposed to both IFNγ and LPS (Fig. 2, *A* and *B*). To see whether stathmin down-regulation was dependent on LPS stimulation, we examined the levels of stathmin and iNOS (1, 48) in IFNγ or LPS alone stimulated macrophages, as well as in resting and classically (IFNγ/LPS)-activated macrophages. LPS-stimulated RAW 264.7 cells exhibited a similarly enhanced iNOS expression as in IFNγ-LPS-activated RAW 264.7 cells, whereas iNOS expression was absent from IFNγ alone stimulated cells (Fig. 2*A*), confirming that IFNγ alone does not activate macrophages (3, 49).

The degradation of stathmin in colorectal cancer cells is mediated by the proteasome (50, 51), so we assessed whether a
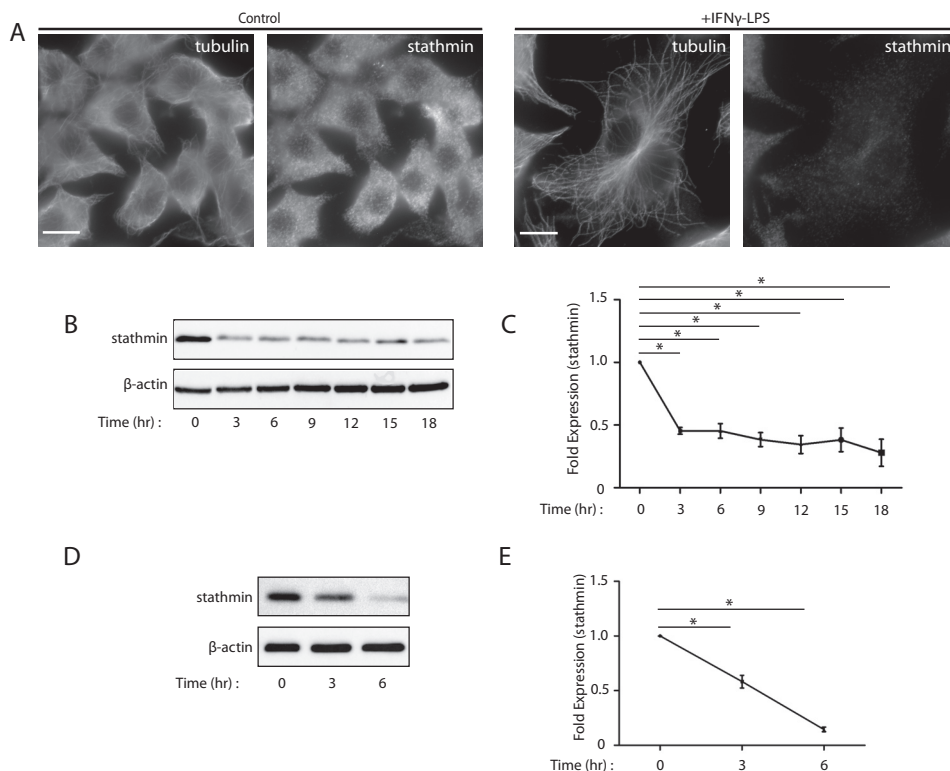
FIGURE 1. **Stathmin protein level is significantly down-regulated in IFNγ-LPS-activated macrophages.** *A,* immunofluorescent imaging analysis revealed altered stathmin expression and MT polymerization in RAW 264.7 cells activated for 6 h with IFNγ-LPS when compared with unstimulated control cells. *B,* immunoblot analysis shows stathmin protein levels in RAW 264.7 cells during the 18-h activation period with IFNγ-LPS. *Top panel,* stathmin expression was detected using a polyclonal anti-stathmin antibody. *Bottom panel,* loading of equal amounts of protein was confirmed using an anti-β-actin antibody. *C,* fold change in stathmin protein levels normalized to β-actin is shown numerically. *D,* immunoblot analysis showing stathmin protein levels in mouse BMDM during 6 h of activation with IFNγ-LPS. *E,* fold decrease in stathmin levels normalized to β-actin is shown relative to unstimulated control cells numerically. The time course was done in triplicate, and data are plotted as the mean ± S.E. from three independent experiments. *, significant fold decrease compared with unstimulated control cells ($p < 0.05$). *Scale bars,* 10 μm.

similar degradation mechanism was at play in activated macrophages. To this end, we measured stathmin protein levels in RAW 264.7 cells that were activated for 3 h prior to an additional 3 h in the presence of 1 μm MG132, a proteasome inhibitor. Cells were lysed at 6 h and subjected to immunoblotting analysis (Fig. 2, *C* and *D*). Stathmin degradation was blocked in the presence of MG132, suggesting a functional proteasome is required for stathmin degradation in IFNγ-LPS-activated macrophages (Fig. 2, *C* and *D*). However, complicating this interpretation was the observation that iNOS protein levels were also severely reduced in MG132-treated cells (Fig. 2*C*), confirming that active proteasomal activity participates in classical activation signaling in macrophages (52).

To overcome issues of impaired macrophage activation upon proteasome inhibition, we looked for other indicators of proteasomal degradation of stathmin. Stathmin degradation by the proteasome is promoted by the phosphorylation of the serine 38 residue on stathmin (53) by either cyclin-dependent kinase 1 (Cdk1) or kinase-interacting stathmin (KIS) (53, 54). Using immunoblotting, we first evaluated the phosphorylation of the serine 38 residue on stathmin in LPS or IFNγ alone and fully activated (IFNγ-LPS) RAW 264.7 cells (Fig. 2*E*). In accordance with the decreased total stathmin levels, an increase in phosphorylated stathmin (Ser-38) was detected in LPS-stimulated and fully activated cells. Serine 38-phosphorylated stathmin was not detected in IFNγ- stimulated and unstimulated cells

(Fig. 2*E*), indicating that the phosphorylation of stathmin was an LPS-dependent response.

The phosphorylation of stathmin at serine 38 is induced by Cdk1 (55, 56), and a study by Liu *et al.* (57) showed a significant up-regulation of Cdk1 in mouse liver cells after LPS exposure. We therefore assessed the expression of Cdk1 in LPS or IFNγ alone stimulated and fully activated RAW 264.7 cells. Total cell lysates were analyzed by immunoblotting (Fig. 2, *E* and *G*). Neither LPS- nor IFNγ-treated cells showed a statistically significant change in Cdk1 expression (Fig. 2*E*), suggesting that total Cdk1 protein levels were not altered during the macrophage activation. Similar results were also obtained from immunoblotting cell lysates with anti-KIS antibodies (data not shown). Cdk1 is activated by phosphorylation of Thr-161 by Cdk-activating kinase and the removal of the inhibitory Thr-14 and Tyr-15 phosphorylations by cdc25B phosphatase (58). To assess Cdk1 activity, we probed lysates of RAW 264.7 cells stimulated with IFNγ-LPS, LPS alone, or IFNγ alone with an antibody against phosphorylated Cdk1 (Thr-161) using immunoblotting (Fig. 2, *E* and *G*). After normalizing to total Cdk1 protein levels, we noticed an increase in Thr-161 phosphorylation of Cdk1 in LPS and IFNγ-LPS-stimulated RAW 264.7 cells, compared with unstimulated cells (Fig. 2, *E* and *G*), which correlate to the enhanced serine 38 phosphorylation of stathmin from earlier experiments (Fig. 2, *E* and *F*). Our experiment thus far suggested that phosphorylation of Cdk1 and stathmin in macrophages was specifically in response to
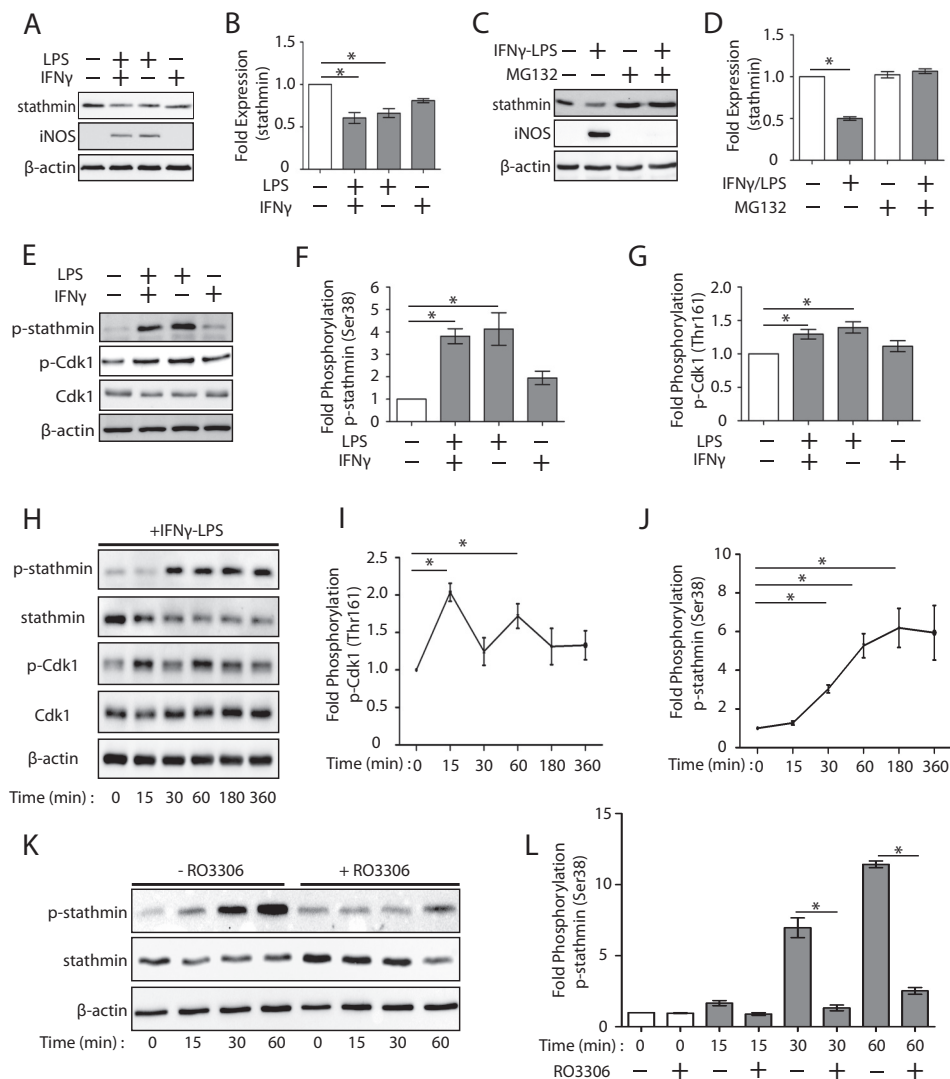
FIGURE 2. **Down-regulation of stathmin is mediated by LPS signaling and requires functional proteasomes and activation of Cdk1.** *A,* immunoblots of stathmin (*top panel*) and iNOS (*middle panel*) expression level during IFNγ-LPS, LPS alone, or IFNγ alone stimulation for 6 h in RAW 264.7 macrophages. β-Actin (*bottom panel*) was used as a loading control. *B,* fold change in stathmin expression following stimulation with IFNγ-LPS, LPS alone, or IFNγ alone was normalized to β-actin and is shown relative to unstimulated control cells. *C,* immunoblot analysis showing the levels of stathmin in resting and activated RAW 264.7 cells in the presence of 10 μM MG132. *D,* fold change in stathmin expression in resting and activated macrophages in the presence or absence of MG132 was normalized to β-actin and is shown numerically relative to unstimulated control cells. *E,* immunoblot analysis of levels of stathmin and Cdk1 phosphorylation in RAW 264.7 cells during activation with IFNγ-LPS. Phospho-stathmin expression was detected using an anti-phospho-stathmin (*Ser-38*) antibody, and phospho-Cdk1 expression was detected using an anti-phospho-Cdk1 (*Thr-161*) antibody. Loading of equal amounts of protein was confirmed using an anti-β-actin antibody. *F,* fold change in phospho-stathmin expression following activation was normalized to total stathmin and is shown relative to unstimulated control cells numerically. *G,* fold change in phospho-Cdk1 expression following activation with IFNγ-LPS was normalized to total Cdk1 and is shown relative to unstimulated control cells numerically. *H,* kinetic analysis of Cdk1 and stathmin phosphorylation in IFNγ-LPS-stimulated macrophages by immunoblotting. RAW 264.7 macrophages were stimulated with IFNγ-LPS for 0, 15, 30, 60, 180, and 360 min. *I* and *J,* rates of Cdk1 and stathmin phosphorylation plotted against total Cdk1 and stathmin level, respectively. Significant fold change compared with unstimulated control cells ($p < 0.05$). *K* and *L,* changes of stathmin phosphorylation by Cdk1 in resting and activated RAW 264.7 macrophages in the presence of 10 μM RO3306 were assessed by immunoblotting. Each experiment was done in triplicate, and data are plotted as the mean ± S.E. from three independent experiments. *, significant fold decrease compared with untreated (−*RO3306*) cells ($p < 0.05$).

extracellular LPS. With respect to kinetics, tyrosine and serine phosphorylations generally occur extremely rapidly during cell signaling (59). Therefore, we investigated the kinetics of LPS-induced Cdk1 and stathmin phosphorylation in activated macrophages at earlier time points. RAW 264.7 macrophages were stimulated with IFNγ-LPS for 0, 15, 30, 60, 180, and 360 min, and the phosphorylation of Cdk1 and stathmin was measured by immunoblotting. As shown in Fig. 2, *H* and *I*, Cdk1 phosphorylation was detected and maximized 15 min after activation; however, total Cdk1 expression was not affected by activation throughout this analysis. Activation-induced stathmin phosphorylation occurred shortly after

Cdk1 phosphorylation at 30 min (Fig. 2, *H* and *I*). Nevertheless, serine 38 residue on stathmin can be regulated by kinases other than Cdk1, including MAPK, KIS, and p38δ kinase (43). To determine whether Cdk1 is responsible for the phosphorylation of stathmin upon macrophage activation, we measured the level of phospho-stathmin (Ser-38) in activated macrophages in the presence of 10 μM RO3306, a well established Cdk1 inhibitor (60). Levels of stathmin phosphorylation following Cdk1 inhibition were then assessed using immunoblotting (Fig. 2, *K* and *L*). After normalizing to total stathmin protein levels, we noticed a significant decrease and delay in stathmin phosphor-
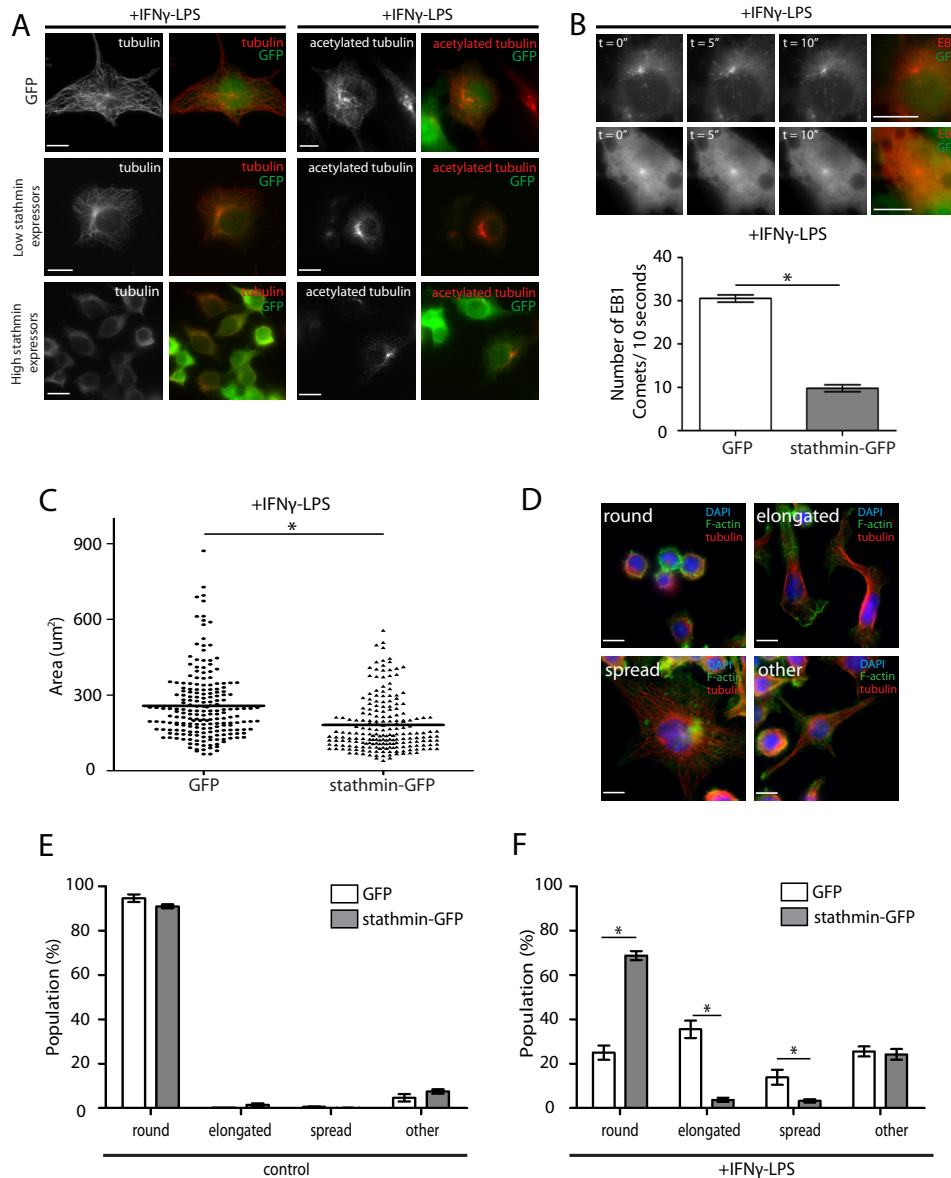
FIGURE 3. **Overexpression of stathmin-GFP in macrophages alters the cytoskeletal and cell morphology changes induced by IFNγ-LPS activation.** *A,* GFP-expressing, low stathmin-GFP-expressing, and high stathmin-GFP-expressing cells were activated for 6 h and immunostained for MTs (*left panel*) and acetylated MTs (*right panel*). *B,* GFP-expressing and stathmin-GFP-expressing cells were transfected with EB1-mCherry (*top panel*) and activated for 6 h, and the time series of EB1-mCherry comets emerging from a centrosome over a period of 10 s were recorded and quantified (*bottom panel*). *C,* quantification of cell spreading in GFP-expressing and stathmin-GFP-expressing cells activated for 6 h. *n* >50 per trial, and five independent experiments were performed. *D,* representative immunofluorescent images for the classification of cell shapes of activated macrophages stained for F-actin (*green*), MTs (*red*), and nuclei (*blue*). *E* and *F,* quantification of cell shapes in control and activated stathmin-GFP-expressing cells, compared with GFP-expressing control cells. *, significant change compared with GFP control cells ($p < 0.05$). Data are plotted as the mean ± S.E. (*error bars*) of results from three independent experiments. *Scale bars*, 10 μm.

ylation in cells treated with RO3306, compared with control untreated cells (Fig. 2L). This finding suggests that Cdk1 is involved in stathmin phosphorylation when macrophages are activated. Overall, our data suggest that Cdk1 activation is induced by LPS signaling to promote the phosphorylation of stathmin and its proteolytic degradation during macrophage activation.

Overexpression of Stathmin Decreases MT Stability and Induces Cell Rounding in IFNγ-LPS-stimulated Macrophages— We next wanted to understand the functional role for stathmin protein reduction in activated macrophages. To circumvent stathmin down-regulation, we created stable cell lines overex-

pressing stathmin-GFP to varying degrees (see "Experimental Procedures"). Low stathmin-GFP, high stathmin-GFP, and GFP alone (control) expressing RAW 264.7 macrophages were stimulated with IFNγ-LPS for 6 h, fixed, and immunostained with either tubulin or acetylated tubulin antibodies and imaged by epifluorescent microscopy (Fig. 3A). High stathmin-GFP overexpressors demonstrated a reduction in MTs compared with low stathmin-GFP and GFP-alone-expressing cells and an increase in "hazy" tubulin staining that likely reflected a larger cytosolic soluble tubulin pool (Fig. 3A, left panel). We have shown that MTs are more stabilized in activated macrophages (19, 25–27), so we next monitored acetylated α-tubulin levels in

Stathmin Reduction in Macrophage Activation

IFNγ-LPS-stimulated macrophages overexpressing stathmin-GFP. Compared with GFP alone cells, high and low stathmin-GFP-overexpressing cells had substantially less acetylated MTs following macrophage activation (Fig. 3A, right panel), suggesting that overexpression of stathmin impacts MT stability. To quantify the impact of stathmin overexpression on MT growth, we used EB1 to measure MT nucleation rate (61). Macrophages stably expressing GFP or stathmin-GFP were transfected with mCherry-tagged EB1. We monitored the number of EB1-mCherry comets emerging from the MTOC over 10 s in activated macrophages (Fig. 3B, top panel). A significant decrease in MT nucleating events was observed in stathmin-GFP-expressing cells, compared with control GFP-expressing cells (Fig. 3B, bottom panel).

Stabilized MTs are required for effective cell spreading, phagocytosis, and matrix metalloproteinase 9 (MMP9) secretion in classically activated macrophages (25, 26). We next examined the ability of activated macrophages to spread when stathmin levels were artificially elevated. Following a 6-h IFNγ-LPS stimulation, stathmin-GFP- and GFP-expressing cells were stained with phalloidin to visualize the F-actin cytoskeleton and demarcate the cell periphery. Quantitative image analysis (see under "Experimental Procedures") of the cell area revealed a significant decrease in cell spreading in stathmin-GFP-expressing cells, compared with control GFP-expressing cells (Fig. 3C). We next determined the impact of stathmin overexpression on activated macrophage morphology. Stathmin-GFP- or GFP-alone-expressing cells were exposed to IFNγ-LPS for 6 h or left unstimulated followed by phalloidin staining and epifluorescence microscopy. For quantification purposes, we classified cells into one of four shaped categories: round, elongated, spread, or other (Fig. 3D). "Round" cells typically had roughly circular cell bodies with minor protrusions; we defined this common phenotype in untreated cells as the resting phenotype. "Elongated" cells had cell bodies that extended into major protrusions positioned along one axis. "Spread" cells expanded in multiple directions and were flatter; both "elongated" and "spread" cell types were defined as activated phenotypes due to their relative prevalence in IFNγ-LPS-treated cells. "Other" cells were those that were ambiguously shaped or did not fit into the previous categories. In unstimulated cells, no significant difference in cell morphologies was observed between stathmin-GFP-expressing and GFP-expressing cell lines (Fig. 3E). The majority of resting macrophages had a round morphology (>90%) with only a small percentage (<10%) of the cell population exhibiting other cell shapes. However, we observed statistically significant differences ($p < 0.05$) in cell morphologies in IFNγ-LPS-activated stathmin-GFP cells compared with GFP-expressing cells, with stathmin-GFP-overexpressing cells showing almost a 3-fold increase in round cells and a 7-fold decrease in the population of cells with morphologies reflecting the activated phenotype (elongated or spread; Fig. 3F). Collectively, overriding the stathmin protein destruction in activated macrophages had pronounced effects on the cytoskeleton and cell shapes, implicating an important role for stathmin down-regulation in the morphological changes that result during macrophage activation.

Stathmin Down-regulation Enhances Dorsal Membrane Ruffle Formation and C3bi-sRBC Binding in Activated Macrophages—Beyond size and shape, dynamic surface events drive the functions of macrophage that include acute protrusions involved in phagocytosis and lamellipodial extensions required for cell mobilization during infection (62, 63). We have previously identified dynamic membrane ruffles as key surface structures in activated macrophages for capturing C3bi-coated particles (19). To evaluate whether stathmin down-regulation in activated macrophages contributes to this process, we monitored dorsal membrane ruffle formation in activated macrophages ectopically overexpressing stathmin-GFP or GFP alone. To evaluate membrane ruffle events, GFP- or stathmin-GFP-expressing cells were activated for 6 h and fixed and processed for F-actin staining and fluorescence. Although the presence of large and complex dorsal membrane ruffles was prominent in GFP-expressing control cells, membrane ruffles were more scarce in stathmin-GFP-overexpressing cells (Fig. 4A, left panel). Quantification of fluorescent images (see under "Experimental Procedures") demonstrated a 50% reduction of elaborate dorsal ruffles in stathmin-GFP-expressing cells compared with control GFP cells (Fig. 4B). Dorsal membrane ruffles are best visualized using SEM (Fig. 4A) (19), so we next analyzed the number of macrophages exhibiting ruffles in IFNγ-LPS-activated GFP versus stathmin-GFP-expressing cells using SEM. Cells were categorized as either "positive" or "negative" depending on the presence or absence of membrane ruffles (Fig. 4C). Quantification of SEM images revealed that the percentage of cells containing one or more ruffles was similar between GFP- and stathmin-GFP-overexpressing macrophages after activation (Fig. 4D), indicating that ruffle formation was not impaired by stathmin-GFP overexpression. However, membrane ruffles were reduced in size and complexity in stathmin-GFP-expressing cells in comparison with GFP-expressing activated macrophages (Fig. 4D). We observed a significant reduction in membrane ruffle length in stathmin-GFP-expressing cells compared with GFP-alone-expressing activated macrophages (Fig. 4E). Together, these data strongly suggest that during macrophage activation, stathmin levels are reduced to enhance membrane ruffle elaboration and maintenance but not to initiate membrane ruffle formation.

We next examined the binding of C3bi-sRBCs to macrophages ectopically overexpressing stathmin, with the hypothesis that reduced membrane ruffle complexity and length may impair the ability of activated macrophage' to capture opsonized targets. RAW 264.7 GFP-expressing and stathmin-GFP stably-expressing cell lines were either stimulated with PMA (15 min) or IFNγ-LPS (6 h) prior to the addition of C3bi-opsonized sRBCs for 10 min followed by fixation and immunostaining for C3bi-sRBCs. PMA induces membrane ruffles in macrophages (64) and was used as a positive control. Stimulation of macrophages with PMA resulted in a significant increase in C3bi-sRBC binding in both GFP- and stathmin-GFP-expressing cells compared with unstimulated cells (Fig. 4F). No significant difference in C3bi-sRBC binding was observed between GFP- versus stathmin-GFP-expressing macrophages when PMA was used as a stimulus (Fig. 4F). Classical activation of macrophages with IFNγ-LPS also resulted in
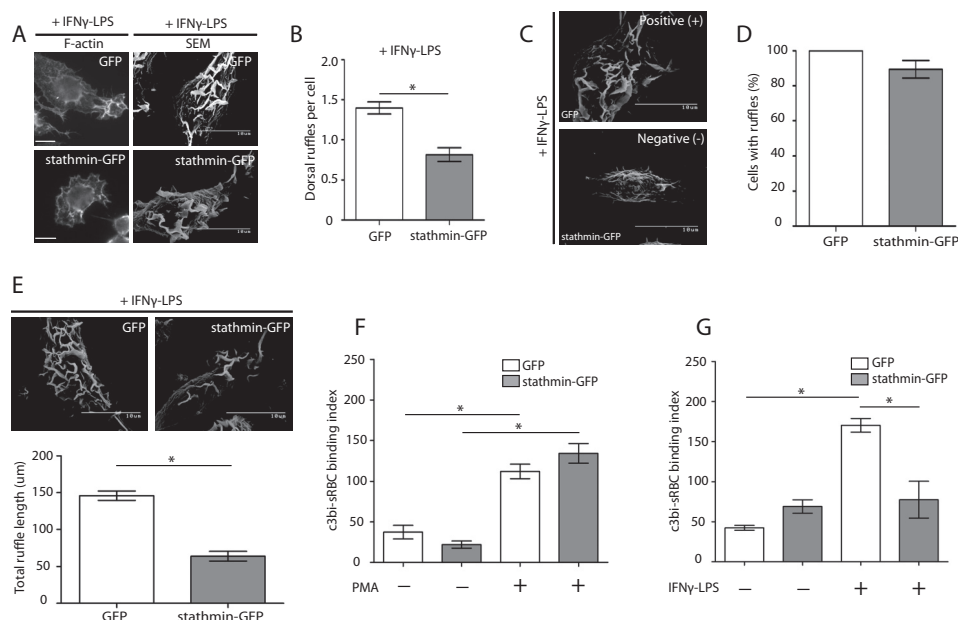
FIGURE 4. **Down-regulation of stathmin is required for membrane ruffle formation and C3bi-opsonized sRBC binding in IFNγ-LPS-activated macrophages.** *A,* representative immunofluorescent and SEM images showing membrane ruffles in IFNγ-LPS-activated GFP-expressing and stathmin-GFP-expressing macrophages. *B,* analysis of immunofluorescent images of dorsal membrane ruffles per cell in IFNγ-LPS-activated stathmin-GFP-expressing cells, compared with GFP-expressing control cells. *C,* representative SEM image for dorsal ruffles in IFNγ-LPS activated GFP-expressing and stathmin-GFP-expressing cells. Presence of ruffling in cells was denoted as positive (+) (presence of ruffle-like membrane protrusions) or negative (−) (absence of ruffle-like membrane protrusions), regardless of ruffle size or morphology. *D,* quantification of cells with ruffles from SEM images in IFNγ-LPS activated stathmin-GFP-expressing and GFP-expressing macrophages. *E,* reduced ruffle length and complexity between activated stathmin-GFP-expressing cells and GFP-expressing cells are shown in a representative SEM image. Quantification of membrane ruffle lengths in activated stathmin-GFP-expressing cells, compared with GFP-expressing cells. *, significant change compared with GFP control group ($p < 0.05$). *F,* determination of the C3bi-sRBC binding index in 100 GFP-expressing or stathmin-GFP-expressing macrophages treated with or without PMA. *, significant change in binding index of PMA-stimulated group compared with unstimulated group ($p < 0.05$). *G,* determination of binding index representing the number of C3bi-sRBCs bound to 100 GFP-expressing or stathmin-GFP-expressing macrophage treated with or without IFNγ-LPS. $n > 500$; *, significant change in binding index of LPS-stimulated group compared with unstimulated group ($p < 0.05$). Data are plotted as the mean ± S.E. *Scale bars*, 10 μm.

a significant increase in C3bi-sRBC binding for GFP- and stathmin-GFP-expressing cells compared with unstimulated cells (Fig. 4*G*). Interestingly, activated macrophages expressing stathmin-GFP had significantly reduced C3bi-sRBC binding, compared with GFP-expressing cells (Fig. 4*G*). These data indicated a unique role for stathmin down-regulation in facilitating ruffle capture in classically activated macrophages.

Down-regulation of Stathmin Protein Is Essential for Full Classical Activation of Macrophages—Our observations so far have demonstrated that preventing stathmin down-regulation in activated macrophages significantly reduced classical activation of phenotypes in these cells, including cell spreading and shape, membrane ruffle elaboration, and C3bi-sRBC binding. Next, we used our stathmin-GFP-stable cells to assess the activation status of these cells in response to IFNγ-LPS stimulation. Stathmin-GFP and GFP-alone stable RAW 264.7 cells were stimulated with IFNγ-LPS for 6 h or left unstimulated (Fig. 5*A*). A GFP antibody confirmed stable expression of the GFP and stathmin-GFP constructs in RAW 264.7 cells. Immunoblotting for stathmin showed an expected decrease in endogenous stathmin in IFNγ-LPS-activated GFP-stable cells, compared with unstimulated GFP cells (Fig. 5*A*). The stathmin-GFP-expressing cells showed bands for both the 48-kDa stathmin-GFP fusion protein as well as the 19-kDa endogenous stathmin. Stathmin-GFP was expressed 5-fold higher than endogenous stathmin (Fig. 5*B, left panel*). In addition, we noticed diminished levels of endogenous stathmin levels upon activation in

stathmin-GFP-overexpressing macrophages (Fig. 5*A*). To assess macrophage activation in these stable cell lines, we analyzed the level of iNOS expression by immunoblotting. Following activation for 6 h, stathmin-GFP-overexpressing cells showed a significant decrease in iNOS protein levels, compared with GFP control cells (Fig. 5*B, right panel*), indicating that stathmin overexpression in macrophages significantly attenuated cellular activation.

Next, we were interested in how stathmin overexpression may influence classical activation signaling. We checked the expression of IκBα in macrophages stimulated with IFNγ-LPS. We found a steady reduction of IκBα expression in GFP-expressing macrophages after activation, with significant IκBα degradation from 15 to 60 min post-stimulation (Fig. 5*C*). It is noteworthy that degradation of IκBα was also observed in stathmin-GFP-expressing macrophages. However, compared with control, the level of IκBα reduction was only significant at 30 min post-activation, and its level recovered shortly thereafter (Fig. 5, *D* and *E*). We next examined the cytoplasmic and nuclear distribution of the NF-κB protein in GFP- and stathmin-GFP-expressing macrophages with or without activation, using confocal microscopy. Cells were activated with IFNγ-LPS for a period of 6 h, fixed, and stained for NF-κB (Fig. 5*F*). For quantification purposes, immunostaining patterns were classified into one of three categories, cytoplasmic, diffuse, or nuclear, based on the localization of NF-κB. In GFP-expressing macrophages, IFNγ-LPS stimulation caused significantly
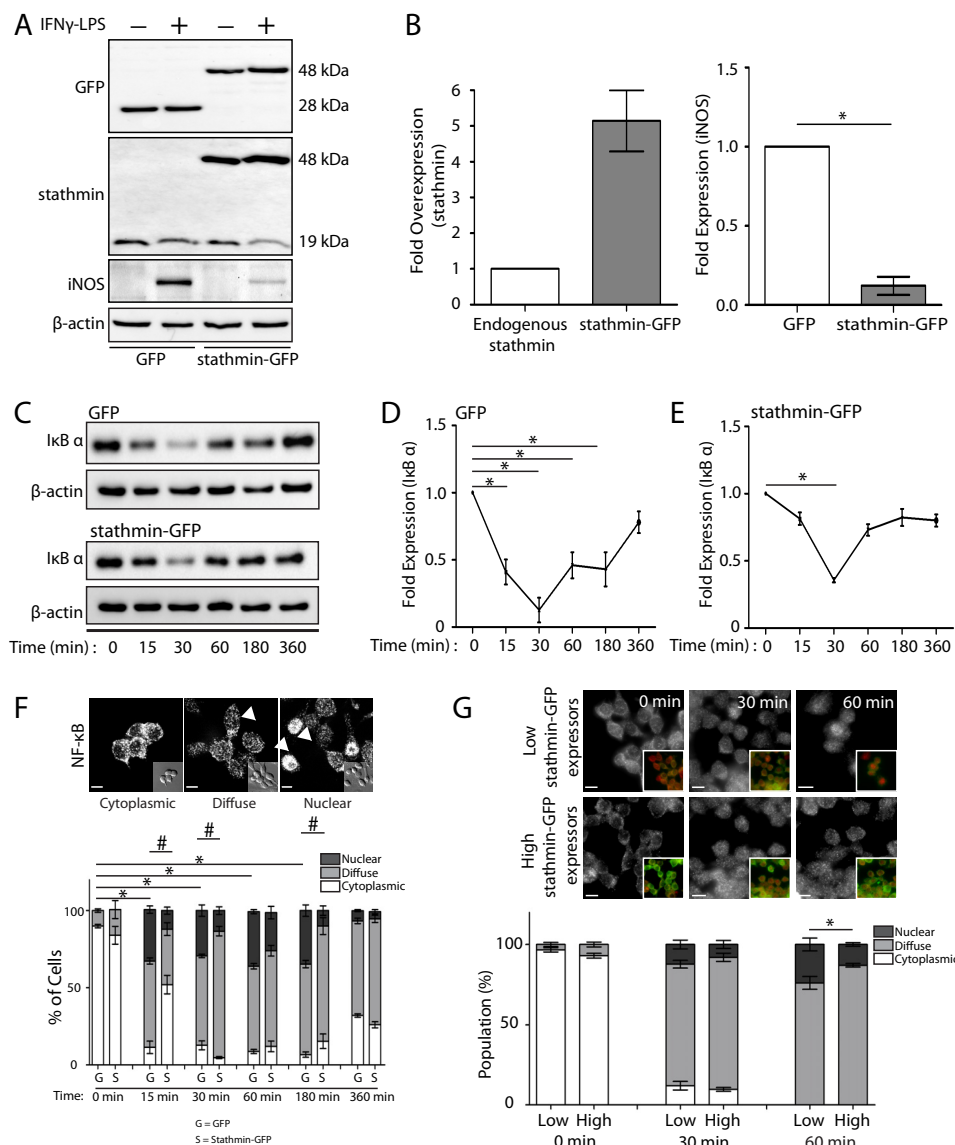
FIGURE 5. **Stathmin overexpression impairs cell activation and IκBα degradation.** *A,* GFP-expressing and stathmin-GFP-expressing macrophages were activated with IFNγ-LPS or left resting. *Top panel,* immunoblotting with an anti-stathmin and anti-GFP antibodies. *Bottom panel,* total iNOS level during activation. β-Actin was used as a loading control. *B,* densitometry quantification of stathmin-GFP (*left panel*) in stathmin-GFP-expressing cells, fold change in stathmin-GFP expression normalized to endogenous stathmin is shown numerically. *, significant fold change compared with endogenous stathmin level ($p < 0.05$). Densitometry quantification of iNOS (*right panel*) levels in activated stathmin-GFP-expressing cells, compared with activated GFP-expressing cells. Fold change in iNOS expression normalized to β-actin is shown numerically. *, significant fold change compared with GFP control cells ($p < 0.05$). *C,* analysis of IκBα expression in IFNγ-LPS-stimulated GFP- and stathmin-GFP-expressing macrophages by immunoblotting. RAW 264.7 macrophages were stimulated with IFNγ-LPS for a defined time period (0, 15, 30, 60, 180, and 360 min). *Top panel,* immunoblot analysis of IκBα expression in GFP-expressing cells. *Bottom panel,* immunoblot analysis of IκBα expression in stathmin-GFP-expressing cells. β-Actin was used as a loading control. *D* and *E,* rates of IκBα degradation plotted against time points post-stimulation. *, significant fold change compared with unstimulated control cells ($p < 0.05$). Data are plotted as the mean ± S.E. from three independent experiments. *F,* analysis of NF-κB distribution in IFNγ-LPS-stimulated GFP and stathmin-GFP-expressing macrophages by confocal microscopy; *arrowheads* indicate nuclear localization of NF-κB. *Top panel,* representative images of three categories of NF-κB distribution in IFNγ-LPS-stimulated cells. *Bottom panel,* quantification of NF-κB distribution in activated GFP and stathmin-GFP-expressing cells. $n > 50$ per trial per time point. *, significant change in nuclear localization compared with unstimulated cells ($p < 0.05$). #, significant change in nuclear localization compared with GFP-expressing cells ($p < 0.05$). *G,* analysis of NF-κB distribution in IFNγ-LPS stimulated low and high stathmin-GFP overexpressors by immunofluorescence microscopy; *arrowheads* indicate nuclear localization of NF-κB. *Top panel,* representative images of NF-κB distribution in IFNγ-LPS-stimulated cells over a period of 60 min. *Bottom panel,* quantification of NF-κB distribution in low and high stathmin-GFP-expressing cells. $n > 50$ per trial per time point. *, significant change in nuclear localization compared with low stathmin-GFP-expressing cells ($p < 0.05$). Data are plotted as the mean ± S.E. from three independent experiments. *Scale bars,* 10 μm.

increased nuclear translocation of NF-κB at 15, 30, 60, and 180 min post-stimulation (Fig. 5*F*), suggesting a sustained activation of inflammatory response genes in these macrophages. However, nuclear translocation of NF-κB in IFNγ-LPS-stimulated stathmin-GFP-overexpressing cells was delayed (Fig. 5*F*). Moreover, low stathmin-GFP overexpressors had significantly

higher nuclear NF-κB distribution than high overexpressors at 60-min post-IFNγ-LPS stimulation (Fig. 5*G*). Collectively, these results suggest that stathmin overexpression prevents full classical activation and nuclear translocation of NF-κB.

Stathmin Down-regulation Regulates TLR4 Surface Display— We next looked more upstream to account for the disrupted
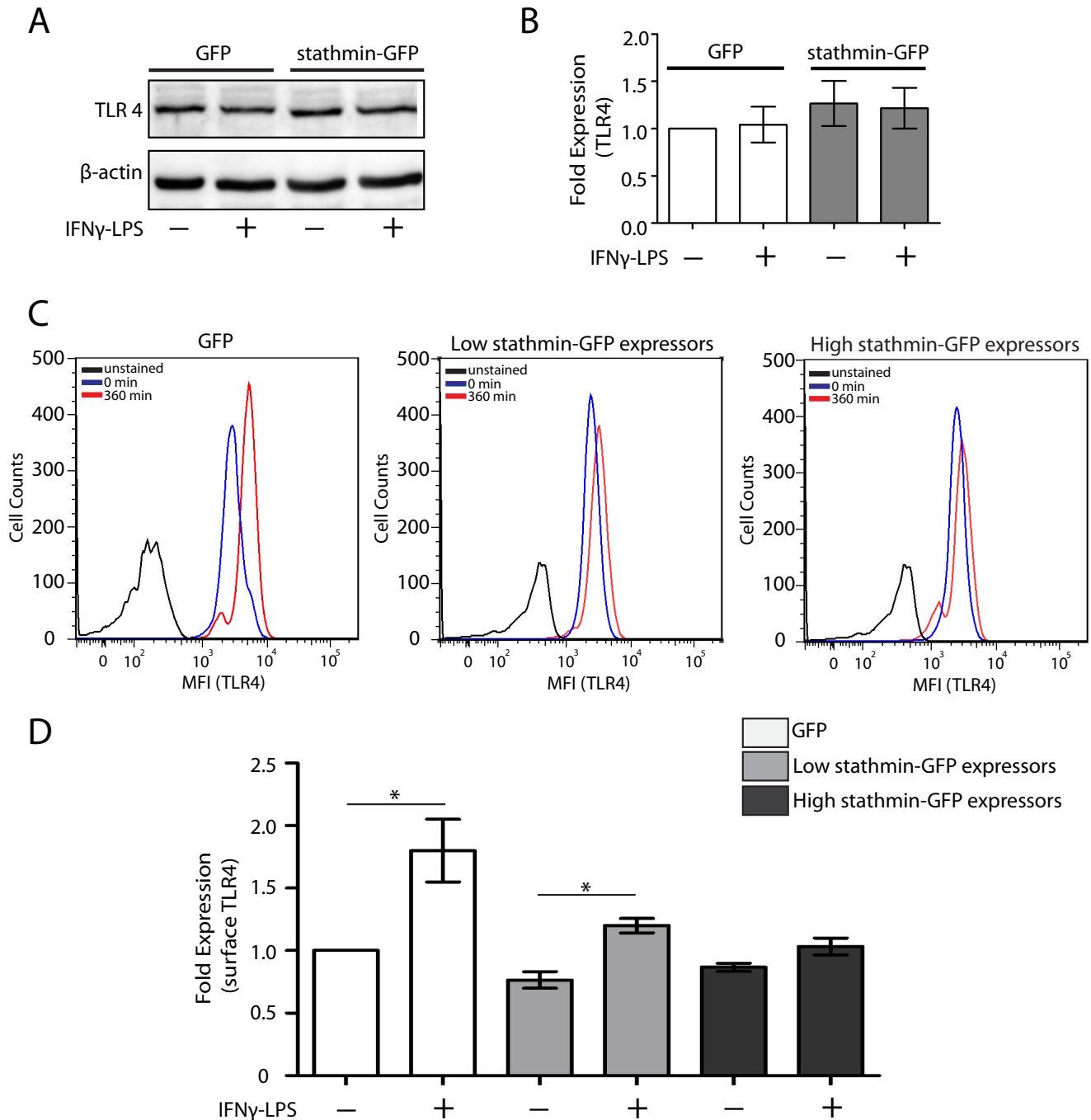
FIGURE 6. **Stathmin down-regulation is required for surface TLR4 expression in resting and activated states.** *A,* immunoblot analysis of TLR4 protein levels after 6 h of IFNγ-LPS activation in GFP-expressing or stathmin-GFP-expressing macrophages. *Top panel*, TLR4 was detected using an anti-TLR4 antibody. *Bottom panel*, loading of equal amounts of protein was confirmed using a β-actin antibody. *B,* expression of total TLR4 between activated GFP-expressing and stathmin-GFP-expressing macrophages is shown by immunoblotting relative to unstimulated control cells. The experiment was done in triplicate, and a representative blot is shown. *C,* surface expression of TLR4 in IFNγ-LPS-stimulated (6 h) and -unstimulated (0 h) GFP-expressing, low stathmin-GFP-, and high stathmin-GFP-overexpressing cells was assessed by flow cytometry using a mAb against surface TLR4. *D,* quantitative evaluation of the relative fluorescent intensity (*RFI*) of TLR4 in GFP-expressing, low stathmin-GFP-, and high stathmin-GFP-expressing cells stimulated or unstimulated with IFNγ-LPS. *, significant fold change compared with unstimulated control cells ($p < 0.05$). Data are plotted as the mean ± S.E. from three independent experiments.

activation in stathmin-GFP-overexpressing cells and examined TLR4 levels and localization in these cells. Total TLR4 protein levels were not altered in stathmin-GFP-overexpressing cells compared with control GFP-expressing macrophages with and without 6 h of IFNγ-LPS stimulation (Fig. 6, *A* and *B*). Immunofluorescent imaging with the TLR4 antibody did not reveal any obvious subcellular differences of TLR4 localization in

stathmin-GFP-expressing cells *versus* control cells (data not shown). To get a more quantitative analysis of cell surface (exposed) TLR4 levels, we turned to flow cytometry analysis. After 6 h of activation with IFNγ-LPS and surface TLR4 staining, a significant increase in surface TLR4 was observed in GFP and low stathmin-GFP-overexpressing macrophages compared with resting cells (Fig. 6, *C, left* and *middle panels,* and *D*). This up-regula-

tion of TLR4 surface display in activated macrophages was abrogated by high stathmin-GFP overexpression (Fig. 6, *C, right panel,* and *D*). These results indicated that overexpression of stathmin disrupts the normal classical activation of macrophages by influencing the levels of the TLR4 receptors on the cell surface of macrophages in a dose-dependent manner.

Discussion

Macrophage activation promotes increased host defense and immune responses. Signals from IFNγ and LPS stimulate a variety of processes in macrophages, and our results suggest that the reduction of stathmin upon activation is critical for cellular activation, morphological changes, and immune functions of macrophages. Stathmin is a potent molecule that can dramatically reduce the cellular MT network, and its protein levels are acutely regulated in activated macrophages (37). We observed a near 50% reduction in stathmin protein levels 3 h after IFNγ-LPS stimulation. Stathmin depletion is key for the extensive MT network changes in mitosis (65). Phosphorylated stathmin levels vary during the cell cycle, and blocking cells in G_1/S for 12 h causes a 20% increase in phosphorylated stathmin (66). Differentiation of megakaryocytes involves stathmin protein reduction, which induces the process of polyploidization. Stathmin mRNA levels show a 50% reduction in levels in megakaryocytes after 6 days of thrombopoietin stimulation (67, 68). Thus, the regulation of stathmin protein levels is pivotal for cell cycle regulation and differentiation, and here we add acute cellular activation to the list. In comparison with the other scenarios, rapid down-regulation of stathmin protein within mere hours in activated macrophages may reflect the urgent need to respond to infections.

We previously reported a significant reduction of stathmin association with MTs in classically activated macrophages (37). Stathmin can be phosphorylated and deactivated by several kinases, including MAPK, calmodulin-dependent protein kinase, and protein kinase A (PKA), and these kinases are thought to modulate the targeting of stathmin to soluble tubulin (43, 69). The inactivation of stathmin by phosphorylation frees tubulin heterodimers from the T_2S complex and creates a local environment that favors MT assembly (43). However, in this study, probing total cell lysates revealed that global stathmin protein levels were lowered, which likely impacted both stathmin subpopulations available for MT binding and cytosolic tubulin sequestration. Additionally, at pH 6.8, stathmin acts as a tubulin-sequestering protein, although at pH 7.5 stathmin stimulates MT plus-end catastrophe (39, 70). However, the cytosolic pH in macrophage is maintained close to physiological conditions (pH 7.2) and does not change upon IFNγ-LPS stimulation (71). Thus, it is likely that the rapid MT stabilization in activated macrophages is achieved through bulk degradation of total stathmin.

Based on our results, stathmin overexpression in macrophages decreased the amount of acetylated MTs, MT nucleation rate, and cell spreading. We observed a similar phenotype when a mutant form of the MT plus-end tracking protein CLIP170 was expressed in activated macrophages, which also destabilized MTs (25). Numerous studies have shown a role for MTs in cell spreading, and there is growing evidence specifically for the stabilized MT subset in this process (72). Stabilized MTs could both structurally expand the base of the cell and/or deliver membrane or adhesion components to facilitate cell spreading (19). In addition to cell spreading, we now demonstrate a critical role for reduced stathmin levels and stabilized MTs in the cell morphology of activated macrophages. We characterized the shapes of macrophages and observed that macrophage activation resulted in an increase in elongated and spread cells. Elongated cells could be indicative of the more migratory and invasive macrophages during inflammation (73), and cell spreading could create a larger surface area for an encounter with pathogens (25). A recent RNAi screen for cell morphologies identified stathmin as an important regulator of cell shape (74), which confirmed earlier work in a human fibrosarcoma cell line (75). Here, we provide detailed cellular phenotypic and ultrastructural evidence to support a key role for stathmin in cell morphology. When we blocked stathmin reduction in activated macrophages by overexpressing stathmin-GFP, the macrophages showed increased rounding and decreased elongation and spreading. The phenotype of unstimulated cells was not altered by stathmin-GFP overexpression, indicating that this is not an artifact of construct overexpression and that the cell shapes of activated macrophages are highly dependent on the destruction of stathmin.

Our previous study showed that CR3-mediated phagocytosis only occurs when membrane ruffles are induced within macrophages by either PMA or IFNγ-LPS stimulation (19, 25). Nocodazole treatment blocked ruffle formation and C3bi-particle binding in both PMA- and IFNγ-LPS-activated macrophages (19, 25); however, stathmin-GFP overexpression only impaired membrane ruffle elaboration and CR3-mediated phagocytosis in IFNγ-LPS-, but not PMA, activated macrophages. The phorbol ester PMA rapidly activates protein kinase C (PKC) to induce membrane ruffles in macrophages and neutrophils (64, 76); however, a role for PKC in membrane ruffle formation induced by IFNγ-LPS has not been elucidated. Our findings could argue that the robust membrane ruffles in PMA-stimulated macrophages are inherently different from those in IFNγ-LPS-activated macrophages. Overexpression of stathmin-GFP drastically reduced acetylated MT formation, which supports an important role for stable MTs in IFNγ-LPS-induced membrane ruffles and C3bi-particle capture. Although we previously showed that the formation of membrane ruffles depends on intact MTs, here we can extend these studies to implicate the stable MT subset.

CLIP-170 is an important contributor to MT stabilization in IFNγ-LPS activated macrophages (25). Interestingly, another MT plus-end-binding protein EB1 binds to stathmin in IGF-1-stimulated breast cancer cells (77). The stathmin-EB1 complex assists in mobilizing WAVE2 to the cell periphery in an MT motor-dependent fashion to elicit membrane ruffle formation (78). Although we observed a marked (>50%) reduction in stathmin levels in activated macrophages, future studies should aim to examine the importance of the persistent/residual stathmin population in mediating macrophage activities, including membrane ruffle formation.

Phagocytosis of large particles requires additional intracellular membrane stores to engulf these particles (79, 80). Focal delivery of intracellular components such as receptors and membranes that are needed for target capture requires the MT
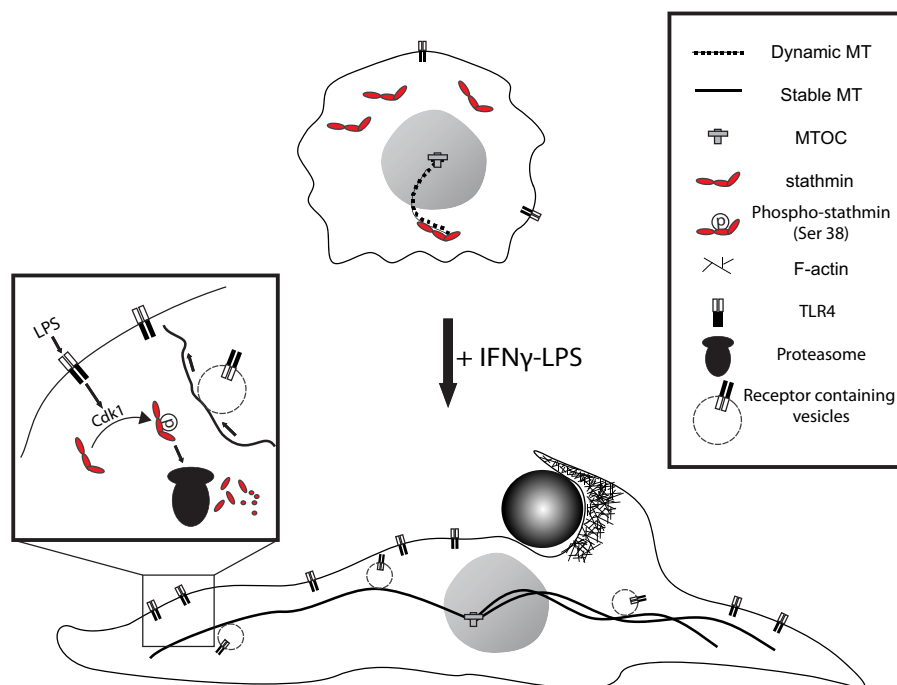
FIGURE 7. Proposed model of stathmin involvement in classical activation of macrophages. Resting macrophages have high levels of stathmin leading to a dynamic MT population. LPS stimulation causes phosphorylation and degradation of stathmin leading to MT stabilization and acetylation. Stabilized MTs promote targeting of TLR4-containing vesicles to the plasma membrane. The potentiated TLR4 signaling causes further stathmin degradation to provoke the full activation phenotype in macrophages, including cell spreading, membrane ruffling, and pathogen capture.

cytoskeleton. We have previously shown that the kinesin, KIF5B, participates in membrane and Fcγ receptor delivery when macrophages are faced with an overload of IgG-opsonized particles (81). We have also shown that MTs are required to deliver CR3 receptors to the cell surface in classically activated macrophages (19). Here, we observe an up-regulation of TLR4 on the cell surface in activated macrophages, which is in agreement with studies on human monocytes (82). We believe that this is an MT-dependent process because of the following: (*a*) stathmin-GFP overexpression and concomitant MT disruption reduce surface TLR4 levels, and (*b*) total TLR4 levels are unaltered after macrophage activation ruling out a biosynthetic contribution to elevated TLR4 on the plasma membrane. It is also possible that stathmin-GFP overexpression affects TLR4 clustering on the cell surface. LPS ligation induces TLR4 clustering on monocytes, and this requires intact F-actin and MT cytoskeletons and is necessary for the formation of functional receptor complexes (83).

Because we observed that acute LPS exposure induces stathmin degradation, the basal levels of surface TLR4 on resting macrophages must be capable of signaling in the absence of the prominent stabilized MT subsets that develop in activated macrophages. In monocytes and macrophages, TLR4 is a highly mobile protein that rapidly and continuously recycles to and from the plasma membrane, until engaged at the surface by LPS (84). Stathmin overexpression did not alter surface TLR4 substantially in resting macrophages; however, it blunts the significant up-regulation of surface TLR4 observed in IFNγ-LPS-stimulated macrophages. Furthermore, less disrupted MT stabilization and surface TLR4 display in cells overexpressing relatively low levels of stathmin-GFP suggest that the amplification of the initial TLR4 signaling is dependent on stabilized

MTs, which participate in continued delivery of TLR4. Thus these newly stabilized MTs act as a positive feedback loop to enhance LPS signaling to promote the full activation phenotype in macrophages (Fig. 7). It was shown recently that MTs are required for targeting TLR4 to membrane ruffles following LPS activation (85). As stathmin overexpression also reduces membrane ruffles on macrophages, both the TLR4 signaling foci within these membrane structures as well as total surface TLR4 levels are impacted when stabilized MTs are diminished. Surface TLR4 expression levels are correlated to the magnitude of the LPS responsiveness (86, 87), and impacting TLR4 surface delivery, recycling, or clustering before and post-activation may explain the altered sensitivity to LPS in stathmin-GFP-overexpressing macrophages. However, it is challenging to completely uncouple MT changes from TLR4 signaling as we observed a recovery of cellular activation in cells overexpressing relatively low levels of stathmin-GFP compared with cells overexpressing high levels of stathmin-GFP. Because the trafficking and membrane targeting of TLR4 relies on MT stabilization (via stathmin down-regulation) in activated macrophages, it is difficult to discriminate whether defects in macrophage activation are due to MT-related mechanisms or low surface TLR4 levels. Future studies will be required to dissect the molecular requirements for MT stabilization on macrophage activation.

Likely influenced by reduced surface TLR4 levels in stathmin-overexpressing macrophages, disrupted NF-κB activation and nuclear translocation explain the diminished activation observed. We saw reduced degradation of IκBα in these cells, which likely accounts for less nuclear NF-κB. Newly synthesized IκBα can terminate the inflammatory signal by entering the nucleus and binding to NF-κB to cause its export to the cytoplasm (88, 89). Thus the rate of IκBα recovery determines

the length of interaction between NF-κB and inflammatory genes. We observed an increased recovery of IκBα levels in stathmin-GFP-transfected cells, which could potentially accelerate the NF-κB export process. Finally, we observed an increased NF-κB nuclear translocation in cells overexpressing relatively low *versus* high levels of stathmin-GFP compared with cells expressing high levels of stathmin-GFP. Cytoskeleton integrity is necessary for the nuclear translocation of NF-κB (90, 91), and stathmin down-regulation in activated macrophages is crucial for the stabilization of MTs. Our results indicate that MT disruption due to stathmin overexpression would expectedly blunt this movement.

In closing, we have revealed a key role for the targeted destruction of stathmin in inducing pronounced MT stabilization in classically activated macrophages. LPS stimulation was the predominant signal for acute reduction of stathmin protein in activated macrophages. Inhibition of Cdk1 activity using RO3306 prevents the phosphorylation of stathmin, indicating that LPS activation of Cdk1 kinase is the major contributing factor for rapid stathmin destruction. Our studies focused on early time points of macrophage classical activation when the major morphological and phenotypic events are occurring. We demonstrate that the classically activated macrophages adopt distinct cell morphologies and that stathmin reduction is required for the phenotypes as well as the subsequent innate immune functions. We previously described a role for stabilized MTs in trafficking MMP9 to the extracellular space (26), and we now implicate these MT subsets in membrane ruffle formation, CR3-mediated phagocytosis, as well as targeting of TLR4 to the cell surface (Fig. 7). Continued signaling through TLR4 is important for NF-κB-mediated gene expression and secretion of pro-inflammatory cytokines in macrophages during a pathogenic challenge (9). Here we show that stathmin can modulate this sustained signaling, likely by affecting the stability of MT to enhance intracellular trafficking of receptor-containing vesicles, MMPs, and cytokines necessary to quickly mount the adaptive immune response.

References

1. Mosser, D. M. (2003) The many faces of macrophage activation. *J. Leukocyte Biol.* **73,** 209–212
2. Mantovani, A., Sica, A., and Locati, M. (2007) New vistas on macrophage differentiation and activation. *Eur. J. Immunol.* **37,** 14–16
3. Pace, J. (1988) Synergistic interactions between IFN-γ and IFN-β in priming murine macrophages for tumor cell killing. *J. Leukocyte Biol.* **520,** 514–520
4. Schletter, J., Heine, H., Ulmer, A. J., and Rietschel, E. T. (1995) Molecular mechanisms of endotoxin activity. *Arch. Microbiol.* **164,** 383–389
5. Ulevitch, R. J., and Tobias, P. S. (1995) Receptor-dependent mechanisms of cell stimulation by bacterial endotoxin. *Annu. Rev. Immunol.* **13,** 437–457
6. Wenzel, R. P., Pinsky, M. R., Ulevitch, R. J., and Young, L. (1996) Current understanding of sepsis. *Clin. Infect. Dis.* **22,** 407–412
7. Takashiba, S., Van Dyke, T. E., Amar, S., Murayama, Y., Soskolne, A. W., and Shapira, L. (1999) Differentiation of monocytes to macrophages primes cells for lipopolysaccharide stimulation via accumulation of cytoplasmic nuclear factor κB. *Infect. Immun.* **67,** 5573–5578
8. Dobrovolskaia, M. A., and Vogel, S. N. (2002) Toll receptors, CD14, and macrophage activation and deactivation by LPS. *Microbes Infect.* **4,** 903–914
9. Kawai, T., and Akira, S. (2007) Signaling to NF-κB by Toll-like receptors. *Trends Mol. Med.* **13,** 460–469
10. Verma, I. M., Stevenson, J. K., Schwarz, E. M., Van Antwerp, D., and Miyamoto, S. (1995) Rel/NF-κB/IκB family: intimate tales of association and dissociation. *Genes Dev.* **9,** 2723–2735
11. O'Dea, E., and Hoffmann, A. (2010) The regulatory logic of the NF-κB signaling system. *Cold Spring Harb. Perspect. Biol.* **2,** a000216
12. Bergqvist, S., Ghosh, G., and Komives, E. A. (2008) The IκBα/NF-κB complex has two hot spots, one at either end of the interface. *Protein Sci.* **17,** 2051–2058
13. Connelly, L., Jacobs, A. T., Palacios-Callender, M., Moncada, S., and Hobbs, A. J. (2003) Macrophage endothelial nitric-oxide synthase autoregulates cellular activation and pro-inflammatory protein expression. *J. Biol. Chem.* **278,** 26480–26487
14. Ghazanfari, T., Yaraee, R., Farahnejad, Z., Rahmati, B., and Hakimzadeh, H. (2010) Macrophages activation and nitric oxide alterations in mice treated with *Pleurotus florida*. *Immunopharmacol. Immunotoxicol.* **32,** 47–50
15. Karupiah, G., Xie, Q. W., Buller, R. M., Nathan, C., Duarte, C., and MacMicking, J. D. (1993) Inhibition of viral replication by interferon-γ-induced nitric-oxide synthase. *Science* **261,** 1445–1448
16. Lane, T. E., Otero, G. C., Wu-Hsieh, B. A., and Howard, D. H. (1994) Expression of inducible nitric-oxide synthase by stimulated macrophages correlates with their antihistoplasma activity. *Infect. Immun.* **62,** 1478–1479
17. MacMicking, J., Xie, Q. W., and Nathan, C. (1997) Nitric oxide and macrophage function. *Annu. Rev. Immunol.* **15,** 323–350
18. Florquin, S., Amraoui, Z., Dubois, C., Decuyper, J., and Goldman, M. (1994) The protective role of endogenously synthesized nitric oxide in staphylococcal enterotoxin B-induced shock in mice. *J. Exp. Med.* **180,** 1153–1158
19. Patel, P. C., and Harrison, R. E. (2008) Membrane ruffles capture C3bi-opsonized particles in activated macrophages. *Mol. Biol. Cell.* **19,** 4628–4639
20. Taylor, P. R., Martinez-Pomares, L., Stacey, M., Lin, H.-H., Brown, G. D., and Gordon, S. (2005) Macrophage receptors and immune recognition. *Annu. Rev. Immunol.* **23,** 901–944
21. Martinez-Pomares, L., and Gordon, S. (2007) Antigen presentation the macrophage way. *Cell* **131,** 641–643
22. Welliver, T. P., Chang, S. L., Linderman, J. J., and Swanson, J. A. (2011) Ruffles limit diffusion in the plasma membrane during macropinosome formation. *J. Cell Sci.* **124,** 4106–4114
23. Ross, G. D., and Větvicka, V. (1993) CR3 (CD11b, CD18): a phagocyte and NK cell membrane receptor with multiple ligand specificities and functions. *Clin. Exp. Immunol.* **92,** 181–184
24. Caron, E., and Hall, A. (1998) Identification of two distinct mechanisms of phagocytosis controlled by different Rho GTPases. *Science* **282,** 1717–1721
25. Binker, M. G., Zhao, D. Y., Pang, S. J., and Harrison, R. E. (2007) Cytoplasmic linker protein-170 enhances spreading and phagocytosis in activated macrophages by stabilizing microtubules. *J. Immunol.* **179,** 3780–3791
26. Hanania, R., Sun, H. S., Xu, K., Pustylnik, S., Jeganathan, S., and Harrison, R. E. (2012) Classically activated macrophages use stable microtubules for matrix metalloproteinase-9 (MMP-9) secretion. *J. Biol. Chem.* **287,** 8468–8483

27. Khandani, A., Eng, E., Jongstra-Bilen, J., Schreiber, A. D., Douda, D., Samavarchi-Tehrani, P., and Harrison, R. E. (2007) Microtubules regulate PI-3K activity and recruitment to the phagocytic cup during Fcγ receptor-mediated phagocytosis in nonelicited macrophages. *J. Leukocyte Biol.* **82,** 417–428

28. Mandelkow, E., and Mandelkow, E. M. (1995) Microtubules and microtubule-associated proteins. *Curr. Opin. Cell Biol.* **7,** 72–81

29. Walczak, C. E. (2000) Microtubule dynamics and tubulin interacting proteins. *Curr. Opin. Cell Biol.* **12,** 52–56

30. Kasas, S., Cibert, C., Kis, A., De Los Rios, P., Riederer, B. M., Forró, L., Dietler, G., and Catsicas, S. (2004) Oscillation modes of microtubules. *Biol. Cell.* **96,** 697–700

31. Hameroff, S. R., and Watt, R. C. (1982) Information processing of microtubules. *J. Theor. Biol.* **98,** 549–561

32. Joshi, H. C. (1998) Microtubule dynamics in living cells. *Curr. Opin. Cell Biol.* **10,** 35–44

33. Bulinski, J. C., Richards, J. E., and Piperno, G. (1988) Posttranslational modifications of α-tubulin: detyrosination and acetylation differentiate populations of interphase microtubules in cultured cells. *J. Cell Biol.* **106,** 1213–1220

34. Fukushima, N., Furuta, D., Hidaka, Y., Moriyama, R., and Tsujiuchi, T. (2009) Post-translational modifications of tubulin in the nervous system. *J. Neurochem.* **109,** 683–693

35. Piperno, G., LeDizet, M., and Chang, X. (1987) Microtubule containing acetylated α-tubulin in mammalian cells in culture. *J. Cell Biol.* **104,** 289–302

36. Bulinski, J. C., and Gundersen, G. G. (1991) Stabilization and post-translational modification of microtubules during cellular morphogenesis. *Bioessays* **13,** 285–293

37. Patel, P. C., Fisher, K. H., Yang, E. C., Deane, C. M., and Harrison, R. E. (2009) Proteomic analysis of microtubule-associated proteins during macrophage activation. *Mol. Cell. Proteomics* **8,** 2500–2514

38. Ozon, S., Guichet, A., Gavet, O., Roth, S., and Sobel, A. (2002) *Drosophila* stathmin: a microtubule-destabilizing factor involved in nervous system formation. *Mol. Biol. Cell* **13,** 698–710

39. Holmfeldt, P., Larsson, N., Segerman, B., Howell, B., Morabito, J., Cassimeris, L., and Gullberg, M. (2001) The catastrophe-promoting activity of ectopic Op18/stathmin is required for disruption of mitotic spindles but not interphase microtubules. *Mol. Biol. Cell* **12,** 73–83

40. Hanash, S. M., Strahler, J. R., Kuick, R., Chu, E. H., and Nichols, D. (1988) Identification of a polypeptide associated with the malignant phenotype in acute leukemia. *J. Biol. Chem.* **263,** 12813–12815

41. Bièche, I., Lachkar, S., Becette, V., Cifuentes-Diaz, C., Sobel, A., Lidereau, R., and Curmi, P. A. (1998) Overexpression of the stathmin gene in a subset of human breast cancer. *Br. J. Cancer* **78,** 701–709

42. Sherbet, G., and Cajone, F. (2005) Stathmin in cell proliferation and cancer progression. *Cancer Genomics Proteomics* **238,** 227–237

43. Cassimeris, L. (2002) The oncoprotein 18/stathmin family of microtubule destabilizers. *Curr. Opin. Cell Biol.* **14,** 18–24

44. Gupta, K. K., Li, C., Duan, A., Alberico, E. O., Kim, O. V., Alber, M. S., and Goodson, H. V (2013) Mechanism for the catastrophe-promoting activity of the microtubule destabilizer Op18/stathmin. *Proc. Natl. Acad. Sci. U.S.A.* **110,** 20449–20454

45. Pustylnik, S., Fiorino, C., Nabavi, N., Zappitelli, T., da Silva, R., Aubin, J. E., and Harrison, R. E. (2013) EB1 levels are elevated in ascorbic acid (AA)-stimulated osteoblasts and mediate cell-cell adhesion-induced osteoblast differentiation. *J. Biol. Chem.* **288,** 22096–22110

46. Iancu-Rubin, C., and Atweh, G. F. (2005) p27(Kip1) and stathmin share the stage for the first time. *Trends Cell Biol.* **15,** 346–348

47. Harvat, B. L., Seth, P., and Jetten, A. M. (1997) The role of p27Kip1 in γ-interferon-mediated growth arrest of mammary epithelial cells and related defects in mammary carcinoma cells. *Oncogene* **14,** 2111–2122

48. Gordon, S. (2003) Alternative activation of macrophages. *Nat. Rev. Immunol.* **3,** 23–35

49. Johnson, H. M., and Torres, B. A. (1985) Mechanism of calcium ionophore A23187-induced priming of bone marrow-derived macrophages for tumor cell killing: relationship to priming by interferon. *Proc. Natl. Acad. Sci. U.S.A.* **82,** 5959–5962

50. Liu, F., Sun, Y.-L., Xu, Y., Liu, F., Wang, L.-S., and Zhao, X.-H. (2013) Expression and phosphorylation of stathmin correlate with cell migration in esophageal squamous cell carcinoma. *Oncol. Rep.* **29,** 419–424

51. Liu, Z., Lu, H., Shi, H., Du, Y., Yu, J., Gu, S., and Chen, X., Liu, K. J., and Hu, C. A. (2005) PUMA overexpression induces reactive oxygen species generation and proteasome-mediated stathmin degradation in colorectal cancer cells. *Cancer Res.* **65,** 1647–1654

52. Qureshi, N., Vogel, S. N., Van Way, C., 3rd, Papasian, C. J., Qureshi, A. A., and Morrison, D. C. (2005) The proteasome. *Immunol. Res.* **31,** 243–260

53. Langenickel, T. H., Olive, M., Boehm, M., San, H., Crook, M. F., and Nabel, E. G. (2008) KIS protects against adverse vascular remodeling by opposing stathmin-mediated VSMC migration in mice. *J. Clin. Invest.* **118,** 3848–3859

54. Zhang, D., Tari, A. M., Akar, U., Arun, B. K., LaFortune, T. A., Nieves-Alicea, R., Hortobagyi, G. N., and Ueno, N. T. (2010) Silencing kinase-interacting stathmin gene enhances erlotinib sensitivity by inhibiting Ser[10] p27 phosphorylation in epidermal growth factor receptor-expressing breast cancer. *Mol. Cancer Ther.* **9,** 3090–3099

55. Beretta, L., Dobránsky, T., and Sobel, A. (1993) Multiple phosphorylation of stathmin. *J. Biol. Chem.* **268,** 20076–20084

56. Belmont, L., Mitchison, T., and Deacon, H. W. (1996) Catastrophic revelations about Op18/stathmin. *Trends Biochem. Sci.* **21,** 197–198

57. Liu, X.-W., Lu, F.-G., Zhang, G.-S., Wu, X.-P., You, Y., Ouyang, C.-H., and Yang, D.-Y. (2004) Proteomics to display tissue repair opposing injury response to LPS-induced liver injury. *World J. Gastroenterol.* **10,** 2701–2705

58. Timofeev, O., Cizmecioglu, O., Settele, F., Kempf, T., and Hoffmann, I. (2010) Cdc25 phosphatases are required for timely assembly of CDK1-cyclin B at the G_2/M transition. *J. Biol. Chem.* **285,** 16978–16990

59. Olsen, J. V., Blagoev, B., Gnad, F., Macek, B., Kumar, C., Mortensen, P., and Mann, M. (2006) Global, *in vivo*, and site-specific phosphorylation dynamics in signaling networks. *Cell* **127,** 635–648

60. Vassilev, L. T., Tovar, C., Chen, S., Knezevic, D., Zhao, X., Sun, H., Heimbrook, D. C., and Chen, L. (2006) Selective small-molecule inhibitor reveals critical mitotic functions of human CDK1. *Proc. Natl. Acad. Sci. U.S.A.* **103,** 10660–10665

61. Piehl, M., Tulu, U. S., Wadsworth, P., and Cassimeris, L. (2004) Centrosome maturation: measurement of microtubule nucleation throughout the cell cycle by using GFP-tagged EB1. *Proc. Natl. Acad. Sci. U.S.A.* **101,** 1584–1588

62. Owen, K. A., Pixley, F. J., Thomas, K. S., Vicente-Manzanares, M., Ray, B. J., Horwitz, A. F., Parsons, J. T., Beggs, H. E., Stanley, E. R., and Bouton, A. H. (2007) Regulation of lamellipodial persistence, adhesion turnover, and motility in macrophages by focal adhesion kinase. *J. Cell Biol.* **179,** 1275–1287

63. Beningo, K. A., and Wang, Y. (2002) Fc-receptor-mediated phagocytosis is regulated by mechanical properties of the target. *J. Cell Sci.* **115,** 849–856

64. Swanson, J. A. (1989) Phorbol esters stimulate macropinocytosis and solute flow-through macrophages. *J. Cell Sci.* **94,** 135–142

65. Rubin, C. I., and Atweh, G. F. (2004) The role of stathmin in the regulation of the cell cycle. *J. Cell. Biochem.* **93,** 242–250

66. Brattsand, G., Marklund, U., Nylander, K., Roos, G., and Gullberg, M. (1994) Cell cycle regulated phosphorylation of oncoprotein 18 on Ser16, Ser25 and Ser-38. *Eur. J. Biochem.* **368,** 359–368

67. Rubin, C. I., French, D. L., and Atweh, G. F. (2003) Stathmin expression and megakaryocyte differentiation: a potential role in polyploidy. *Exp. Hematol.* **31,** 389–397

68. Iancu-Rubin, C., Gajzer, D., Tripodi, J., Najfeld, V., Gordon, R. E., Hoffman, R., and Atweh, G. F. (2011) Down-regulation of stathmin expression is required for megakaryocyte maturation and platelet production. *Blood* **117,** 4580–4589

69. Lin, X., Tang, M., Tao, Y., Li, L., Liu, S., Guo, L., Li, Z., Ma, X., Xu, J., and Cao, Y. (2012) Epstein-Barr virus-encoded LMP1 triggers regulation of the ERK-mediated Op18/stathmin signaling pathway in association with cell cycle. *Cancer Sci.* **103,** 993–999

70. Howell, B., Deacon, H., and Cassimeris, L. (1999) Decreasing oncoprotein 18/stathmin levels reduces microtubule catastrophes and increases microtubule polymer *in vivo*. *J. Cell Sci.* **112,** 3713–3722

71. Swallow, C. J., Grinstein, S., and Rotstein, O. D. (1992) Lipopolysaccharide impairs macrophage cytoplasmic pH regulation under conditions simulating the inflammatory microenvironment. *J. Leukocyte Biol.* **52,** 395–399

72. Tran, A. D., Marmo, T. P., Salam, A. A., Che, S., Finkelstein, E., Kabarriti, R., Xenias, H. S., Mazitschek, R., Hubbert, C., Kawaguchi, Y., Sheetz, M. P., Yao, T.-P., and Bulinski, J. C. (2007) HDAC6 deacetylation of tubulin modulates dynamics of cellular adhesions. *J. Cell Sci.* **120,** 1469–1479

73. Pixley, F. J. (2012) Macrophage migration and its regulation by CSF-1. *Int. J. Cell Biol.* **2012,** 501962

74. Yin, Z., Sadok, A., Sailem, H., McCarthy, A., Xia, X., Li, F., Garcia, M. A., Evans, L., Barr, A. R., Perrimon, N., Marshall, C. J., Wong, S. T., and Bakal, C. (2013) A screen for morphological complexity identifies regulators of switch-like transitions between discrete cell shapes. *Nat. Cell Biol.* **15,** 860–871

75. Belletti, B., Nicoloso, M. S., Schiappacassi, M., Berton, S., Lovat, F., Wolf, K., Canzonieri, V., D'Andrea, S., Zucchetto, A., Friedl, P., Colombatti, A., and Baldassarre, G. (2008) Stathmin activity influences sarcoma cell shape, motility, and metastatic potential. *Mol. Biol. Cell.* **19,** 2003–2013

76. Downey, G. P., Chan, C. K, Lea, P., Takai, A., and Grinstein, S. (1992) Phorbol ester-induced actin assembly in neutrophils: role of protein kinase C. *J. Cell Biol.* **116,** 695–706

77. Morimura, S., and Takahashi, K. (2011) Rac1 and stathmin but not EB1 are required for invasion of breast cancer cells in response to IGF-I. *Int. J. Cell Biol.* **2011,** 615912

78. Takahashi, K., Tanaka, T., and Suzuki, K. (2010) Directional control of WAVE2 membrane targeting by EB1 and phosphatidylinositol 3,4,5-triphosphate. *Cell. Signal.* **22,** 510–518

79. Cannon, G. J., and Swanson, J. A. (1992) The macrophage capacity for phagocytosis. *J. Cell Sci.* **101,** 907–913

80. Touret, N., Paroutis, P., Terebiznik, M., Harrison, R. E., Trombetta, S., Pypaert, M., Chow, A., Jiang, A., Shaw, J., Yip, C., Moore, H.-P., van der Wel, N., Houben, D., Peters, P. J., de Chastellier, C., *et al.* (2005) Quantitative and dynamic assessment of the contribution of the ER to phagosome formation. *Cell* **123,** 157–170

81. Silver, K. E., and Harrison, R. E. (2011) Kinesin 5B is necessary for delivery of membrane and receptors during FcγR-mediated phagocytosis. *J. Immunol.* **186,** 816–825

82. Gomes, N. E., Brunialti, M. K., Mendes, M. E., Freudenberg, M., Galanos, C., and Salomão, R. (2010) Lipopolysaccharide-induced expression of cell surface receptors and cell activation of neutrophils and monocytes in whole human blood. *Braz. J. Med. Biol. Res.* **43,** 853–858

83. Dai, Q., Zhang, J., and Pruett, S. B. (2005) Ethanol alters cellular activation and CD14 partitioning in lipid rafts. *Biochem. Biophys. Res. Commun.* **332,** 37–42

84. Latz, E., Visintin, A., Lien, E., Fitzgerald, K. A., Monks, B. G., Kurt-Jones, E. A., Golenbock, D. T., and Espevik, T. (2002) Lipopolysaccharide rapidly traffics to and from the Golgi apparatus with the toll-like receptor 4-MD-2-CD14 complex in a process that is distinct from the initiation of signal transduction. *J. Biol. Chem.* **277,** 47834–47843

85. Luo, L., Wall, A. A., Yeo, J. C., Condon, N. D., Norwood, S. J., Schoenwaelder, S., Chen, K. W., Jackson, S., Jenkins, B. J., Hartland, E. L., Schroder, K., Collins, B. M., Sweet, M. J., and Stow, J. L. (2014) Rab8a interacts directly with PI3Kγ to modulate TLR4-driven PI3K and mTOR signalling. *Nat. Commun.* **5,** 4407

86. Tsukamoto, H., Fukudome, K., Takao, S., Tsuneyoshi, N., Ohta, S., Nagai, Y., Ihara, H., Miyake, K., Ikeda, Y., and Kimoto, M. (2013) Reduced surface expression of TLR4 by a V254I point mutation accounts for the low lipopolysaccharide responder phenotype of BALB/c B cells. *J. Immunol.* **190,** 195–204

87. Kalis, C., Kanzler, B., Lembo, A., Poltorak, A., Galanos, C., and Freudenberg, M. A. (2003) Toll-like receptor 4 expression levels determine the degree of LPS-susceptibility in mice. *Eur. J. Immunol.* **33,** 798–805

88. Cheong, R., Hoffmann, A., and Levchenko, A. (2008) Understanding NF-κB signaling via mathematical modeling. *Mol. Syst. Biol.* **4,** 192

89. Birbach, A., Gold, P., Binder, B. R., Hofer, E., de Martin, R., and Schmid, J. A. (2002) Signaling molecules of the NF-κ B pathway shuttle constitutively between cytoplasm and nucleus. *J. Biol. Chem.* **277,** 10842–10851

90. Spencer, W., Kwon, H., Crépieux, P., Leclerc, N., Lin, R., and Hiscott, J. (1999) Taxol selectively blocks microtubule dependent NF-κB activation by phorbol ester via inhibition of IkBa phosphorylation and degradation. *Oncogene* **18,** 495–505

91. Mackenzie, G. G., Keen, C. L., and Oteiza, P. I. (2006) Microtubules are required for NF-κB nuclear translocation in neuroblastoma IMR-32 cells: modulation by zinc. *J. Neurochem.* **99,** 402–415